Vibrationally State-Resolved Rotational Relaxation Time

Y. Yun[1] and E. Kustova[1]
St Petersburg University, 7-9 Universitetskaya Embankment, St Petersburg, Russia, 199034

(*Electronic mail: st135205@student.spbu.ru.)

(*Electronic mail: e.kustova@spbu.ru.)

(Dated: 15 August 2025)

In high-temperature non-equilibrium flows, the traditional Parker rotational relaxation model based on the rigid rotor assumption fails to accurately describe the effects of internal molecular structure on the energy transfer processes, creating a critical bottleneck for precise modeling. This study aims to establish an improved computational framework for rotational relaxation times that incorporates vibrational state-resolved calculations and rovibrational coupling effects to overcome fundamental limitations of existing simplified models. Based on the Variable Soft Sphere molecular model and Statistical Inelastic Cross Section theory, an exponential correlation function was introduced to accurately describe transition probabilities between rotational energy levels, establishing a complete state-to-state rotational relaxation time computational model. Through systematic parameter sensitivity analysis, a strict linear relationship between averaged rotational relaxation time and the model parameter θ' was discovered, significantly streamlining the parameter fitting procedure. For N_2-N_2, N_2-N and O_2-O_2, O_2-O systems, optimal θ' values were determined with average relative errors below 0.7% when validated against recent theoretical data. Important computational guidelines were established. The improved model provides theoretically accurate and computationally efficient tools for transport coefficient calculations in hypersonic flow numerical simulations, with significant implications for engineering applications such as atmospheric reentry and interplanetary exploration.

I. INTRODUCTION

With the rapid development of aerospace technology, hypersonic vehicles are playing an increasingly important role in atmospheric reentry, interplanetary exploration, and other fields[1?] . Under hypersonic flight conditions, gas molecules undergo complex nonequilibrium phenomena under the influence of strong shock waves[2], which directly affect the stability and safety of the vehicles[3,4]. Among the numerous nonequilibrium processes, rotational energy relaxation is one of the key physical mechanism[5,6]. The rotational relaxation time determines the characteristic time scale required for molecular rotational energy to reach equilibrium. When it is comparable to the flow characteristic time, the rotational mode cannot equilibrate rapidly, thus leading to the occurrence of rotational nonequilibrium phenomena[7,8]. These rotational nonequilibrium effects have extensive and profound impacts: they not only alter shock wave structures and thermodynamic properties[9,10], but also influence chemical reaction rates[11], ultimately causing significant changes in the macroscopic characteristics of the entire flow field, including critical parameters such as shock standoff distance, wall heat flux, and aerodynamic force distribution[12,13]. Furthermore, rotational relaxation time serves as the foundation for calculating transport coefficients such as viscosity and thermal conductivity[14–16], and the accurate prediction of these transport properties is crucial for the reliability of flow field numerical simulations[17,18].

The traditional Parker model[19] is based on the rigid rotor assumption, making it difficult to accurately describe the effects of internal molecular structure and rovibrational coupling on the energy transfer processes under high-temperature conditions. In the state-to-state kinetic theory, each vibrationally excited state of a molecule requires the introduction of corresponding rotational relaxation times[14], but experimental data for such relaxation times are currently unavailable. With increasing computational resources, methods based on *ab initio* potential energy surfaces have been applied[20–22]. In Ref. 13, complete state-to-state transition rates containing 9,390 rovibrational states from the NASA Ames database were used to construct comprehensive master equation systems describing bound-bound, bound-free, and predissociation transition processes for studying rotational relaxation in N_2-N collisions. In Ref. 9, an innovative atomistic quasi-classical trajectory (QCT) approach is employed, separating rotational and vibrational energy modes based on *ab initio* N_3 potential energy surfaces to calculate rotational relaxation times for N_2-N and N_2-N_2 collisions. Venturi et al.[23] adopted a rovibrational state-resolved QCT method, using nine potential energy surfaces developed by Varga et al. to describe multiplet interactions in the O_2-O system. However, these approaches face extremely high computational costs, particularly for molecule-molecule collision types, where the need to handle more than 10^{15} collision pair combinations makes complete rovibrational state-to-state calculations practically infeasible in real applications. Bechina and Kustova[5] developed a statistical inelastic collision cross-section calculation method suitable for Direct Simulation Monte Carlo (DSMC) methods, based on the Variable Soft Sphere (VSS) molecular model and Statistical Inelastic Cross Section (SICS) model by Koura[24]. They simplified the calculation of rotational relaxation processes by assuming constant transition probabilities between rotational energy levels and applied this to collision cross-section calculations for different rotational levels in N_2-N interactions. However, they employed simplified assumptions such as statistical uncorrelation, neglecting the exponential decay law of transition probabilities between rotational energy levels with energy gaps. While this dramatically reduced computational costs, it caused results to deviate from true values.

The main contribution of this study is the establishment of a complete improved computational method for rotational relaxation times, including both atom-molecule and molecule-molecule collisions, and achieving vibrational state-resolved rotational relaxation time calculations for nitrogen and oxygen molecular systems. By introducing exponential correlation functions to describe the variation of transition probabilities between rotational states with energy gaps, the limitations of traditional simplified models are overcome. Compared to complete state-to-state calculations that require handling 10^{15} rovibrational state combinations, the improved model in this work significantly reduces computational complexity while maintaining physical description accuracy, making precise modeling of important collision types such as N_2-N, N_2-N_2, O_2-O, and O_2-O_2 feasible under ordinary computational resource conditions.

The structure of this paper is as follows: Section II establishes the theoretical model framework, including the state-to-state approach of the Chapman-Enskog method, Parker model, simplified statistical rotational relaxation time model, and improved rotational relaxation time model. Section III systematically compares the performance differences between simplified and improved models through parameter sensitivity analysis and validation, determines optimal model parameters, and establishes parameter fitting methods. Section IV presents detailed computational results for collision integrals and rotational relaxation times, with comprehensive comparison and validation against existing theoretical data. Section V summarizes the main research conclusions and contributions. Through this systematic study, important theoretical foundations and computational tools are provided for precise modeling of hypersonic non-equilibrium flows.

II. THEORETICAL MODELS

A. State-to-state approach

In the state-to-state approximation[14] of the Chapman-Enskog method, elastic collisions and rotational energy transitions in a gas mixture are classified as fast processes. Under this assumption, the hierarchy of characteristic times is given by the following relation:

$$\tau_{\text{el}} \lesssim \tau_{\text{rot}} \ll \tau_{\text{vibr}} < \tau_{\text{react}} \sim \theta^*, \tag{1}$$

where τ_{el}, τ_{rot}, τ_{vibr}, τ_{react} represent the relaxation times of translational, rotational, and vibrational degrees of freedom, and the characteristic time of chemical reactions, respectively. θ^* is the characteristic time of variation of the macroscopic parameters of the gas.

The state-to-state model, applicable under conditions where vibrational and chemical relaxation rates are similar in magnitude to the evolution rates of macroscopic flow parameters, generates the following coupled transport equations[14]:

$$\frac{\mathrm{d}n_{ci}}{\mathrm{d}t} + n_{ci}\nabla\cdot\mathbf{v} + \nabla\cdot(n_{ci}\mathbf{V}_{ci}) = R_{ci}, \qquad i = 0,\ldots,L_c, \quad c = 1,\ldots,L, \tag{2}$$

$$\rho\frac{d\mathbf{v}}{dt} = -\nabla\cdot\mathbf{P}, \tag{3}$$

$$\rho\frac{dU}{dt} = -\nabla\cdot\mathbf{q} - \mathbf{P}:\nabla\mathbf{v}, \tag{4}$$

where n_{ci}, $\mathbf{V}_{ci}$, R_{ci} are the number density, diffusion velocity and production rate of molecules of species c at vibrational level i respectively, R_{ci} describes the change in the number density due to coupled vibrational energy transitions and chemical reactions, L is the number of chemical species in the mixture, L_c is the number of vibrationally excited state for molecular species c, ρ is the mass density of the gas mixture, $\mathbf{v}$ is the flow velocity, t is the time, $\mathbf{P}$ is the pressure tensor, U is the specific total energy, $\mathbf{q}$ is the total energy flux.

The first-order approximations of the generalized Chapman-Enskog method yield the following constitutive equations for diffusion velocities, the stress tensor, and heat flux[14]:

$$\mathbf{V}_{ci} = -\sum_{dk} D_{cidk}\mathbf{d}_{dk} - D_{T_{ci}}\nabla\ln T, \tag{5}$$

$$\mathbf{P} = (p - p_{\text{rel}})\mathrm{I} - 2\eta\mathrm{S} - \zeta\nabla\cdot\mathbf{v}\mathrm{I} \tag{6}$$

$$\mathbf{q} = -\lambda'\nabla T - p\sum_{ci} D_{T_{ci}}\mathbf{d}_{ci} + \sum_{ci}\left(\frac{5}{2}k_BT + \langle\varepsilon_j^{ci}\rangle_{\text{rot}} + \varepsilon_i^c + \varepsilon_c\right)n_{ci}\mathbf{V}_{ci}, \tag{7}$$

where D_{cidk} and $D_{T_{ci}}$ represent the diffusion and thermal diffusion coefficients specific to the vibrational states, $p = nk_BT$ is the pressure, n is the number density of a gas mixture, k_B is the Boltzmann constant, T is the temperature; p_{rel} denotes the relaxation pressure, η is the shear viscosity coefficient, ζ is the bulk viscosity coefficient, λ' is the partial thermal conductivity coefficient, $\mathbf{I}$ is the unit tensor, $\mathbf{S}$ is the rate-of-shear tensor, and $\mathbf{d}_{dk}$ refers to the diffusive driving forces. Furthermore, ε_i^c is the vibrational energy of the ith level for molecular species c, ε_j^{ci} is the rotational energy of the jth level for molecular species c at the ith vibrational energy level, ε_c is the formation energy; the notation $\langle\ldots\rangle_{\text{rot}}$ means averaging over rotational states with the local equilibrium Boltzmann distribution.

For the rotational energy ε_j^{ci}, the non-rigid rotator model is employed that considers the dependence of rotational energy on the vibrational energy level of rotating molecules:

$$\frac{\varepsilon_j^{ci}}{hc} = B_i^c j(j+1) - D_i^c j^2(j+1)^2 + \ldots, \tag{8}$$

where h is the Planck constant ($h = 6.6261\times10^{-34}$ J·s), c is the speed of light, j is the rotational energy level of the molecule, B_e^c, D_e^c, α_e^c, and β_e^c are spectroscopic constants.

For the vibrational energy ε_i^c we use the anharmonic oscillator model:

$$\frac{\varepsilon_i^c}{hc} = \omega_e^c\left(i+\frac{1}{2}\right) - \omega_e^c x_e^c\left(i+\frac{1}{2}\right)^2 + \omega_e^c y_e^c\left(i+\frac{1}{2}\right)^3 + \ldots, \tag{9}$$

where ω_e^c, $\omega_e^c x_e^c$, and $\omega_e^c y_e^c$ are spectroscopic constants characterizing the vibrational frequency and its anharmonicity.

For the transport coefficients calculation, the first-order distribution functions is expanded into the series in the Sonine and Waldmann–Trübenbacher polynomials; the transport coefficients are expressed in terms of the expansion coefficients, which, in turn, are found as solutions of transport linear systems[14]. For instance, the thermal conductivity coefficient λ' is expressed in terms of expansion coefficients $a_{ci,rp}$:

$$\lambda' = \sum_{ci} \frac{5}{4} k_B \frac{n_{ci}}{n} a_{ci,10} + \sum_{ci} \frac{m_c}{2} \frac{n_{ci}}{n} c_{\mathrm{rot},ci} a_{ci,01}, \tag{10}$$

where m_c is the mass of molecular species c, and the specific heat of rotational degrees of freedom is defined as:

$$c_{\mathrm{rot},ci} = \left(\frac{\partial E_{\mathrm{rot},ci}}{\partial T} \right)_V, \tag{11}$$

$$\begin{aligned} E_{\mathrm{rot},ci} &= \frac{1}{m_c Z_{ci}^{\mathrm{rot}}} \sum_j s_j^{ci} \varepsilon_j^{ci} \exp\left(-\frac{\varepsilon_j^{ci}}{k_B T} \right), \\ Z_{ci}^{\mathrm{rot}} &= \sum_j s_j^{ci} \exp\left(-\frac{\varepsilon_j^{ci}}{k_B T} \right). \end{aligned} \tag{12}$$

Here, $E_{\mathrm{rot},ci}$ is the specific rotational energy for molecule c at the ith vibrational level, Z_{ci}^{rot} is the rotational partition function.

For the total rotational specific heat, the following relation is satisfied:

$$c_{\mathrm{rot}} = \sum_{ci} \frac{\rho_{ci}}{\rho} c_{\mathrm{rot},ci}. \tag{13}$$

In order to calculate the expansion coefficients $a_{ci,rp}$ in Eq. (10), linear transport systems are derived, which include the bracket integrals linked to the linearized collision operator of rapid processes; the bracket integrals can be further reduced to the $\Omega_{cidk}^{(l,r)}$ collision integrals and relaxation times[14]. The algorithm for the calculation of other transport coefficients is basically similar, although the resulting transport systems and bracket integrals are different.

Each internal energy level is treated as a distinct species in the state-to-state approach, and the macroscopic conservation laws are extended accordingly. Above equations describe the evolution of molecular energy states in non-equilibrium gas flows and provide a framework for investigating complex gas dynamics involving internal energy modes such as vibration, rotation, and chemical reactions. In the present work, the collision cross sections and rotational relaxation times for each vibrational state are calculated, and the internal energy variations are analyzed on a state-to-state basis.

TABLE I. collision parameters for different systems.

System	ω	c	ζ_c^∞	E_c^*, J	θ_R, K
N_2-N	0.275	240.3×10^{-20}	20.3898	1.15127×10^{-21}	2.86256
N_2-N_2	0.235	216.1×10^{-20}	20.3898	1.34655×10^{-21}	2.86256
O_2-O	0.199	114.7×10^{-20}	20.8478	1.22331×10^{-21}	2.05706
O_2-O_2	0.201	155.6×10^{-20}	20.8478	1.48282×10^{-21}	2.05706

B. Parker model

In the calculation of rotational relaxation time, it is commonly assumed that the system is quiescent[25], and therefore

$$\tau_{\mathrm{rot}} = \left. \frac{E_r^0}{\frac{dE_r(t)}{dt}} \right|_{E_r=0}, \tag{14}$$

where $E_r(t)$ is the energy of rotational degrees of freedom per unit volume, and E_r^0 is the equilibrium value of this energy. The Parker model[19] adopts the same assumptions as Eq. (14) and defines the number of collisions as follows:

$$\zeta_c^{\mathrm{rot}} = \frac{\zeta_c^\infty}{F_c(T)}, \tag{15}$$

with the function $F_c(T)$ given by:

$$\begin{aligned} F_c(T) = 1 &+ \frac{\pi^{3/2}}{2} \left(\frac{k_B T}{E_c^*} \right)^{-1/2} + \left(\frac{\pi^2}{4} + 2 \right) \left(\frac{k_B T}{E_c^*} \right)^{-1} \\ &+ \pi^{3/2} \left(\frac{k_B T}{E_c^*} \right)^{-3/2}. \end{aligned} \tag{16}$$

Here E_c^* is the well-depth value of the intermolecular potential energy for species c, ζ_c^∞ is the limiting value of ζ_c, they are given in Table I.

The expression for the rotational relaxation time for molecular species c is as follows:

$$\tau_c^{\mathrm{rot}} = \frac{\zeta_c^{\mathrm{rot}} \pi \eta_c}{4p}, \tag{17}$$

where η_c is the effective viscosity coefficient of c species. This equation indicates that the rotational relaxation time based on the Parker model does not account for the effect of the molecular vibrational state on the relaxation process, highlighting the need for a more refined formulation.

C. Simplified state-to-state rotational relaxation time model

The VSS molecular model for inverse power-law and Lennard-Jones potentials, developed by Koura and Matsumoto[26], maintains computational efficiency comparable to the Variable Hard Sphere (VHS) model while providing superior accuracy in multicomponent gas simulations. The VSS model enables for more physically realistic representation of

momentum and energy-transfer mechanisms during molecular interactions.

In their seminal work, Koura [24] implemented a comprehensive approach using the VSS model to address elastic collisions, while complementing it with the SICS model for rotationally inelastic collisions. This integrated methodology established a rigorous statistical inelastic collision cross-section model applicable to DSMC methodologies. The equations in the above paper introduce a simplification in the rotational relaxation process based on the statistical uncorrelated assumption, whereby the transition probabilities between rotational energy states are treated as constants.

Based on this theoretical foundation, Bechina and Kustova [5] extended the analysis to compute collision cross sections of different rotational levels for N_2-N interactions. The expressions for the simplified statistical rotationally inelastic cross section are given below.

The molecular collisions are characterized by the total collision cross section:

$$\sigma_{\text{tot}}(jl,\varepsilon) = \sum_{j'l'} \sigma_{jj',ll'}(\varepsilon) = \sigma_{jj,ll}(\varepsilon) + \sigma_{\text{inel}}(jl,\varepsilon), \quad (18)$$

where ε is the relative collisional energy, $\sigma_{jj',ll'}(\varepsilon)$ is the inelastic cross section for molecules transitioning from initial rotational states j, l to final rotational states j', l', $\sigma_{jj,ll}(\varepsilon)$ is the elastic cross section for colliding molecules with internal states j, l remaining unchanged during the collision, $\sigma_{\text{inel}}(jl,\varepsilon)$ is the total inelastic collision. The units are m^2.

The total inelastic collision cross section can be written in the form

$$\sigma_{\text{inel}}(jl,\varepsilon) = \sum_{j'l}^{*} \sigma_{jj',ll'}(\varepsilon), \quad (19)$$

where $\sum_{j'l'}^{*}$ denotes the summation over all rotational levels j', l' except j, l.

Combining Eqs. (18) and (19), we obtain:

$$\sigma_{\text{inel}}(jl,\varepsilon) = \sum_{j'l'} \sigma_{jj',ll'}(\varepsilon) - \sigma_{jj,ll}(\varepsilon). \quad (20)$$

The elastic collision cross section weakly depends on the rotational state[27]. If we assume the elastic collision cross section independent of the internal state, we can use the VSS model[26] for its evaluation:

$$\sigma_{jj,ll}(\varepsilon) = \sigma_{\text{el}}(\varepsilon) = c(\varepsilon/k_B)^{-\omega}, \quad (21)$$

the parameters c and ω are standard literature values from Koura and Matsumoto [28] and are given in Table I. These parameters were derived for air species in the temperature range 300–15,000 K.

The relationship between $\sigma_{\text{el}}(\varepsilon)$ and $\sigma_{jj',ll'}(\varepsilon)$ is assumed to be given by the statistical form[24]:

$$\sigma_{jj',ll'}(\varepsilon) / \sigma_{\text{el}}(\varepsilon) = \xi_{j'l'}(E) S_{jj',ll'}(E). \quad (22)$$

Here $\xi_{j'l'}(E)$ represents uncorrelated function of total collision energy $E = \varepsilon + \varepsilon_i^c + \varepsilon_j^{ci} + \varepsilon_k^d + \varepsilon_l^{dk}$ and satisfies the condition $\xi_{j'l'}(E) = 0$ for $E \le \varepsilon_{j'}^{ci} + \varepsilon_{l'}^{dk}$; $S_{jj',ll'}(E)$ is the correlation function. The uncorrelated function $\xi_{j'l'}(E)$ is defined by:

$$\xi_{j'l'}(E) = C(E) s_{j'}^{ci} s_{l'}^{dk} \left(E - \varepsilon_{j'}^{ci} - \varepsilon_{l'}^{dk}\right) \sigma_{\text{el}} \left(E - \varepsilon_{j'}^{ci} - \varepsilon_{l'}^{dk}\right), \quad (23)$$

$$\xi_{jl}(E) = C(E) s_j^{ci} s_l^{dk} \left(E - \varepsilon_j^{ci} - \varepsilon_l^{dk}\right) \sigma_{\text{el}} \left(E - \varepsilon_j^{ci} - \varepsilon_l^{dk}\right). \quad (24)$$

with the condition $\sigma_{\text{el}} \left(E - \varepsilon_{j'}^{ci} - \varepsilon_{l'}^{dk}\right) = 0$ for $E \le \varepsilon_{j'}^{ci} + \varepsilon_{l'}^{dk}$. In the above equations, the statistical weight of the j'th rotational level is given by $s_{j'}^{ci} = 2j' + 1$. The function $C(E)$ is equal to a constant value for a given total energy E and determined for rotationally inelastic collision using the Parker's classical rotational energy gain function:

$$C(E) = \frac{2\Delta E_R(E)}{G_R(E)}. \quad (25)$$

The function $G_R(E)$, defined by summing over discrete rotational energy levels:

$$G_R(E) = \sum_{jl} (\varepsilon_j^{ci} + \varepsilon_l^{dk}) s_j^{ci} s_l^{dk} (E - \varepsilon_j^{ci} - \varepsilon_l^{dk}) \sigma_{\text{el}}(E - \varepsilon_j^{ci} - \varepsilon_l^{dk}), \quad (26)$$

$\Delta E_R(E)$ represents the rotational energy gain during a collision, and it is given by:

$$\Delta E_R(E) = \left[\frac{E}{2} + \frac{2\pi}{3}(EE^*)^{1/2} + \left(\frac{\pi^2}{4} + 2\right) E^*\right] / \zeta_c^{\infty}. \quad (27)$$

Substituting Eq. (22) into Eq. (20), we obtain the inelastic collision in the form:

$$\sigma_{\text{inel}}(jl,\varepsilon) = \xi(E) \sigma_{\text{el}}(\varepsilon) - \xi_{jl}(E) S_{jj,ll}(E) \sigma_{\text{el}}(\varepsilon)$$
$$\xi(E) = \sum_{j'l'} \xi_{j'l'}(E) S_{jj',ll'}(E). \quad (28)$$

Substituting Eqs. (23), (25), (26) into Eq. (28), the inelastic rotational collision cross section can be written as:

$$\sigma_R(jl,\varepsilon)=\left[\sum_{j'l'}\frac{2\Delta E_R(E)s_j^{ci}s_{l'}^{dk}\left(E-\varepsilon_{j'}^{ci}-\varepsilon_{l'}^{dk}\right)\sigma_{\rm el}(E-\varepsilon_{j'}^{ci}-\varepsilon_{l'}^{dk})}{\sum_{jl}(\varepsilon_j^{ci}+\varepsilon_l^{dk})s_j^{ci}s_l^{dk}(E-\varepsilon_j^{ci}-\varepsilon_l^{dk})\sigma_{\rm el}(E-\varepsilon_j^{ci}-\varepsilon_l^{dk})}S_{jj',ll'}(E)-\frac{2\Delta E_R(E)s_j^{ci}s_l^{dk}\left(E-\varepsilon_j^{ci}-\varepsilon_l^{dk}\right)\sigma_{\rm el}\left(E-\varepsilon_j^{ci}-\varepsilon_l^{dk}\right)}{\sum_{jl}(\varepsilon_j^{ci}+\varepsilon_l^{dk})s_j^{ci}s_l^{dk}(E-\varepsilon_j^{ci}-\varepsilon_l^{dk})\sigma_{\rm el}(E-\varepsilon_j^{ci}-\varepsilon_l^{dk})}\right]\sigma_{\rm el}(\varepsilon). \tag{29}$$

In the simplified statistical rotational inelastic cross section model, the following assumptions are considered: (1) The rotational energy of the jth level is assumed as rigid rotator model $\varepsilon_j^{ci}=\varepsilon_j^c=k_B\theta_R j(j+1)$, θ_R is the characteristic rotational temperature in K and given in Table I. (2) The summation of $\sum_{j'l'}\xi_{j'l'}(E)$ is approximated by the integration ($\theta_R \ll E/k_B$). (3) The correlation function $S_{jj',ll'}(E)=1$.

Based on above assumptions, the classical forms of $G_R(E)$ and $\xi(E)$ are simplified from the summation form to:

$$G_{R,\rm simp}(E)=\left\{c/[2(2-\omega)(3-\omega)(4-\omega)(k_B\theta_R)^2]\right\}E^{4-\omega}, \tag{30}$$

$$\xi_{\rm simp}(E)=\sum_{j'l'}\xi_{j'l'}(E)=(4-\omega)\frac{\Delta E_R(E)}{E}. \tag{31}$$

In $\xi_{jl}(E)$, a simplified form $G_{R,\rm simp}(E)$ is also adopted, so $\xi_{jl}(E)$ becomes:

$$\xi_{jl,\rm simp}(E)=\frac{2\Delta E_R(E)s_j^{ci}s_l^{dk}\left(E-\varepsilon_j^{ci}-\varepsilon_l^{dk}\right)\sigma_{\rm el}\left(E-\varepsilon_j^{ci}-\varepsilon_l^{dk}\right)}{\left\{c/[2(2-\omega)(3-\omega)(4-\omega)(k_B\theta_R)^2]\right\}E^{4-\omega}}. \tag{32}$$

The total rotational cross section with uncorrelated function is simplified as:

$$\sigma_{R,\rm simp}(jl,\varepsilon)=\left[\xi_{\rm simp}(E)-\xi_{jl,\rm simp}(E)\right]\sigma_{\rm el}(\varepsilon). \tag{33}$$

In the state-to-state approximation, it is assumed that rotational and vibrational energy changes do not occur simultaneously during a collision. Accordingly, the rotational relaxation time for a molecule of species c in the ith vibrational state colliding with a molecule of species d in the kth vibrational state is given by[14]:

$$\frac{1}{\tau_{cidk}^{\rm rot}}=\frac{4k_Bn}{m_cc_{{\rm rot},ci}}\left\langle\Delta\mathscr{E}_{ci}^{\rm rot}\Delta\mathscr{E}_{cidk}^{\rm rot}\right\rangle_{cidk}, \tag{34}$$

If the collision partner is an atom, Eq.(34) simplifies to:

$$\frac{1}{\tau_{ci}^{\rm rot}}=\frac{4k_Bn}{m_cc_{{\rm rot},ci}}\left\langle\left(\Delta\mathscr{E}_{ci}^{\rm rot}\right)^2\right\rangle_{ci}. \tag{35}$$

In the above equations, the dimensionless rotational energy variation upon collision $\Delta\mathscr{E}_{cidk}^{\rm rot}$ is determined as follows[14]:

$$\Delta\mathscr{E}_{cidk}^{\rm rot}=\Delta\mathscr{E}_{ci}^{\rm rot}+\Delta\tilde{\mathscr{E}}_{dk}^{\rm rot}, \tag{36}$$

$$\Delta\mathscr{E}_{ci}^{\rm rot}=\frac{\varepsilon_{j'}^{ci}-\varepsilon_j^{ci}}{k_BT},\quad \Delta\tilde{\mathscr{E}}_{dk}^{\rm rot}=\frac{\varepsilon_{l'}^{dk}-\varepsilon_l^{dk}}{k_BT}. \tag{37}$$

Within the state-to-state approximation, the averaging operator is defined in the form:

$$\langle F\rangle_{cidk}=\left(\frac{k_BT}{2\pi m_{cd}}\right)^{1/2}\sum_{jlj'l'}\frac{s_j^{ci}s_l^{dk}}{Z_{ci}^{\rm rot}Z_{dk}^{\rm rot}}\times\int F_{cij}\gamma^3\exp\left(-\gamma^2-\mathscr{E}_j^{ci}-\mathscr{E}_l^{dk}\right)\sigma_{cd,ijkl}^{j'l'}d^2\Omega\,d\gamma, \tag{38}$$

where $m_{cd}=m_cm_d/(m_c+m_d)$ is the reduced collision mass for particles of the cth and dth species, F_{cij} is an arbitrary function of velocity, $\gamma=\left[(m_{cd}/(2k_BT))^{1/2}g\right]$is the reduced relative velocity, g is the relative velocity, $\mathscr{E}_j^{ci}=\varepsilon_j^{ci}/(k_BT)$is the dimensionless rotational energy, $\sigma_{cd,ijkl}^{j'l'}$ is cross section with rotational energy transitions, and $d^2\Omega$ is the solid angle, within which the relative velocity vector is located after collision.

Taking into account that $\iint\sigma_{cd,ijkl}^{j'l'}(\gamma,\chi,\varepsilon)\sin\chi\,d\chi\,d\varepsilon=\sigma_R(jl,\varepsilon)$, the rotational relaxation time can be written as:

$$\frac{1}{\tau_{cidk}^{\rm rot}}=\frac{4k_Bn}{m_cc_{{\rm rot},ci}}\left(\frac{k_BT}{2\pi m_{cd}}\right)^{1/2}\sum_{jj'll'}\frac{s_j^{ci}s_l^{dk}}{Z_{ci}^{\rm rot}Z_{dk}^{\rm rot}}\Delta\mathscr{E}_{ci}^{\rm rot}\Delta\mathscr{E}_{cidk}^{\rm rot}\times e^{-\mathscr{E}_j^{ci}-\mathscr{E}_l^{dk}}\int_{\gamma_{\min}}^{\infty}\gamma^3e^{-\gamma^2}\sigma_R(jl,\varepsilon)\,d\gamma,, \tag{39}$$

the summation is carried out using the rule

$$\sum_{jj'll'}=\sum_{j=0}^{N_{{\rm rot},i}-1}\sum_{\substack{j'=j-\Delta j\\ j'\geq0}}\sum_{l=0}^{N_{{\rm rot},k}-1}\sum_{\substack{l'=l-\Delta l\\ l'\geq0}}^{l+\Delta l\leq N_{{\rm rot},k}-1}, \tag{40}$$

and

$$\Delta\mathscr{E}_{ci}^{\rm rot}\Delta\mathscr{E}_{cidk}^{\rm rot}=(\mathscr{E}_{j'}^{ci}-\mathscr{E}_j^{ci})(\mathscr{E}_{j'}^{ci}-\mathscr{E}_j^{ci}+\mathscr{E}_{l'}^{dk}-\mathscr{E}_l^{dk}). \tag{41}$$

For multi-quantum rotational energy transitions, $j'=j\pm\Delta j$, $\Delta j=2,4,6,\ldots$ for homonuclear molecules and $\Delta j=1,2,3,\ldots$ for heteronuclear molecules. $N_{{\rm rot},j}$ is the number of rotational energy levels for a molecule on the ith vibrational level. The value $\gamma_{\min}$ is related to j and j'. If $j'<j$, then $\gamma_{\min}=0$. If $j'>j$, $\gamma_{\min}=\sqrt{(\mathscr{E}_{j'}^{ci}-\mathscr{E}_j^{ci})}$.

It is also convenient to introduce the collision integral for rotational energy transfer Q_r in the form:

$$Q_r=\left(\frac{k_BT}{2\pi m_{cd}}\right)^{1/2}\sum_{jj'll'}\frac{s_j^{ci}s_l^{dk}}{Z_{ci}^{\rm rot}Z_{dk}^{\rm rot}}\Delta\mathscr{E}_{ci}^{\rm rot}\Delta\mathscr{E}_{cidk}^{\rm rot}e^{-\mathscr{E}_j^{ci}-\mathscr{E}_l^{dk}}\times\int_{\gamma_{\min}}^{\infty}\gamma^3e^{-\gamma^2}\sigma_R(jl,\varepsilon)\,d\gamma. \tag{42}$$

This integral corresponds to the integral $\Omega^{(0,0)}_{cidk}$[14] occurring in the expressions for the bracket integrals required for the calculation of transport coefficients and reaction rates.

Since $\varepsilon = k_B T\gamma^2$, then when using simplified statistical rotational inelastic cross section, $\sigma_{R,\mathrm{simp}}(jl,\varepsilon) = \left[\xi_{\mathrm{simp}}(E) - \xi_{jl,\mathrm{simp}}(E)\right]\sigma_{el}(\varepsilon)$, the simplified vibrationally state-resolved rotational relaxation time can be obtained as:

$$\frac{1}{\tau^{\mathrm{rot}}_{cidk,\mathrm{simp}}} = \frac{4k_B n}{m_c c_{\mathrm{rot},ci}}\left(\frac{k_B T}{2\pi m_{cd}}\right)^{1/2}\sum_{jj'll'}\frac{s^{ci}_j s^{dk}_l}{Z^{\mathrm{rot}}_{ci}Z^{\mathrm{rot}}_{dk}}\Delta\mathscr{E}^{\mathrm{rot}}_{ci}\Delta\mathscr{E}^{\mathrm{rot}}_{cidk} \times e^{-\mathscr{E}^{ci}_j-\mathscr{E}^{dk}_l}\int_{\gamma_{\min}}^{\infty}\gamma^3 e^{-\gamma^2}\sigma_{R,\mathrm{simp}}(jl,\varepsilon)d\gamma. \tag{43}$$

When the collision partner is an atom, Eq.(43) simplifies to:

$$\frac{1}{\tau^{\mathrm{rot}}_{ci,\mathrm{simp}}} = \frac{4k_B n}{m_c c_{\mathrm{rot},ci}}\left(\frac{k_B T}{2\pi m_{cd}}\right)^{1/2}\sum_{jj'}\frac{s^{ci}_j}{Z^{\mathrm{rot}}_{ci}} \times\left(\mathscr{E}^{ci}_{j'}-\mathscr{E}^{ci}_j\right)^2 e^{-\mathscr{E}^{ci}_j}\int_{\gamma_{\min}}^{\infty}\gamma^3 e^{-\gamma^2}\sigma_{R,\mathrm{simp}}(jl,\varepsilon)d\gamma. \tag{44}$$

The integral parts in above formulas cannot be calculated analytically, so they are taken by using 15-point Gauss-Kronrod quadratures.

D. Improved state-to-state rotational relaxation time model

In the simplified rotational relaxation time model, ignoring the correlation between forward and backward transitions of quantum rotational energy levels, a rigid body model is used in the simplification process of $G_R(E)$ and $\xi(E)$, which means that the rotational energy of the molecule is independent of vibrational energy levels. To improve the computational accuracy, this subsection aims to establish a more refined mathematical model independent of the aforementioned assumptions.

In the improved rotational relaxation time model, the calculation of the elastic collision cross section still uses the VSS model, however with the following difference: (1) $\xi(E)$ cannot be simplified into a classical form. (2) The correlation function $S_{jj',ll'}(E)$ is considered to be a function of the total collision energy and transition energy. In Section III we will analyze the impact of the classical form of $G_R(E)$ on the computational results.

In Koura's work[24], it was mentioned that the correlation function can be represented through either the exponential gap model or the power law gap model. In 1972, Polanyi and Woodall[29] investigated the mechanism of rotational relaxation and tested four different models, among which only the exponential model could adequately describe the observed relaxation patterns, while the other models failed to accurately reproduce the experimental data. In Alexander's early work[25], the validity of these two models was verified, and it was pointed out that the exponential gap model has more comprehensive theoretical support and formal derivation. In the present work, calculations were performed for both the exponential gap model and the power law gap model, but the fitting results of the power law gap model showed significant deviation from the reference values. Additionally, considering the limited space, this paper only presents the relevant formulas and calculation procedures for the exponential gap model. The form of the correlation function $S_{jj',ll'}(E)$ is as follows:

$$S_{jj',ll'}(E) = \exp\left(-\theta\left|\Delta E\right|\right). \tag{45}$$

Here $\Delta E = \varepsilon^{ci}_{j'} + \varepsilon^{dk}_{l'} - \varepsilon^{ci}_j - \varepsilon^{dk}_l$ is energy transition gap. $\theta = \theta'/E$ is the function of E, the parameter θ' does not have a universal analytical form, as it varies depending on the gas type and collision partner. Parameters for the exponential transition probability model can be obtained by fitting existing experimental or other research data. This paper also uses similar method to obtain the parameter θ'.

Due to the consideration of the correlation function, the function $\xi(E)$ related to the correlation function cannot be written in a simplified form, and we need to express it in the following form:

$$\xi_{\mathrm{imp}}(E) = \sum_{j'l'}\xi_{j'l'}(E)S_{jj',ll'}(E) = \sum_{j'l'}\frac{2\Delta E_R(E)s^{ci}_j s^{dk}_{l'}(E-\varepsilon^{ci}_{j'}-\varepsilon^{dk}_{l'})\sigma_{\mathrm{el}}(E-\varepsilon^{ci}_{j'}-\varepsilon^{dk}_{l'})\exp(-\theta'|\Delta E|/E)}{\sum_{jl}(\varepsilon^{ci}_j+\varepsilon^{dk}_l)s^{ci}_j s^{dk}_l(E-\varepsilon^{ci}_j-\varepsilon^{dk}_l)\sigma_{\mathrm{el}}(E-\varepsilon^{ci}_j-\varepsilon^{dk}_l)}, \tag{46}$$

$$\xi_{jl,\mathrm{imp}}(E) = \frac{2\Delta E_R(E)s^{ci}_j s^{dk}_l(E-\varepsilon^{c}_j-\varepsilon^{d}_l)\sigma_{\mathrm{el}}(E-\varepsilon^{ci}_j-\varepsilon^{dk}_l)}{\sum_{jl}(\varepsilon^{ci}_j+\varepsilon^{dk}_l)s^{ci}_j s^{dk}_l(E-\varepsilon^{ci}_j-\varepsilon^{dk}_l)\sigma_{\mathrm{el}}(E-\varepsilon^{ci}_j-\varepsilon^{dk}_l)}. \tag{47}$$

Based on above equations, the improved total rotational cross section is given by:

$$\sigma_{R,\mathrm{imp}}(jl,\varepsilon) = \left[\xi_{\mathrm{imp}}(E) - \xi_{jl,\mathrm{imp}}(E)\right]\sigma_{\mathrm{el}}(\varepsilon). \tag{48}$$

When considering the correlation function, the improved rotational relaxation time can be obtained as:

$$\frac{1}{\tau^{\mathrm{rot}}_{cidk,\mathrm{imp}}} = \frac{4k_B n}{m_c c_{\mathrm{rot},ci}}\left(\frac{k_B T}{2\pi m_{cd}}\right)^{1/2}\sum_{jj'll'}\frac{s^{ci}_j s^{dk}_l}{Z^{\mathrm{rot}}_{ci}Z^{\mathrm{rot}}_{dk}}\Delta\mathscr{E}^{\mathrm{rot}}_{ci}\Delta\mathscr{E}^{\mathrm{rot}}_{cidk} \times e^{-\mathscr{E}^{ci}_j-\mathscr{E}^{dk}_l}\int_{\gamma_{\min}}^{\infty}\gamma^3 e^{-\gamma^2}\left[\xi_{\mathrm{imp}}(E) - \xi_{jl,\mathrm{imp}}(E)\right]\sigma_{\mathrm{el}}(\varepsilon)\,d\gamma. \tag{49}$$

When the collision partner is an atom, Eq.(47) simplifies to:

$$\frac{1}{\tau^{\text{rot}}_{ci,\text{imp}}} = \frac{4k_B n}{m_c c_{\text{rot},ci}} \left(\frac{k_B T}{2\pi m_{cd}}\right)^{1/2} \sum_{jj'} \frac{s^{ci}_j}{Z^{\text{rot}}_{ci}} \left(\mathscr{E}^{ci}_{j'} - \mathscr{E}^{ci}_{j}\right)^2 e^{-\mathscr{E}^{ci}_j} \times \int_{\gamma_{\min}}^{\infty} \gamma^3 e^{-\gamma^2} \left[\xi_{\text{imp}}(E) - \xi_{j,\text{imp}}(E)\right] \sigma_{\text{el}}(\varepsilon)\, d\gamma. \tag{50}$$

Furthermore, in order to compare the rotational energy relaxation time in the present work with other researchers' results, we use the state-resolved relaxation time averaged over the vibrational energy:

$$\frac{c_{\text{rot},c}}{\tau^{\text{rot}}_{cdk}} = \frac{1}{Z^{\text{vibr}}_c} \sum_i e^{-\mathscr{E}^c_i} \frac{c_{\text{rot},ci}}{\tau^{\text{rot}}_{cidk}}, \tag{51}$$

$$\frac{c_{\text{rot},d}}{\tau^{\text{rot}}_{cd}} = \frac{1}{Z^{\text{vibr}}_d} \sum_k e^{-\mathscr{E}^d_k} \frac{c_{\text{rot},dk}}{\tau^{\text{rot}}_{cdk}}, \tag{52}$$

When the collision partner is an atom, Eq.(50) simplifies to:

$$\frac{c_{\text{rot},c}}{\tau^{\text{rot}}_{c}} = \frac{1}{Z^{\text{vibr}}_c} \sum_i e^{-\mathscr{E}^d_i} \frac{c_{\text{rot},ci}}{\tau^{\text{rot}}_{ci}}, \tag{53}$$

where Z^{vibr}_c is the partition function of vibrational degrees of freedom for a molecule of the cth species.

III. PARAMETER SENSITIVITY ANALYSIS AND VALIDATION

The theoretical framework established in Section II introduces a refined methodology for calculating rotational relaxation times by incorporating vibrational states and exponential correlation functions. To evaluate the accuracy and applicability of the proposed improved model relative to the simplified model in specific systems, this section presents a systematic comparison and validation using the N_2–N, N_2–N_2, O_2–O and O_2–O_2 systems as the subject.

In the simplified model, we used the $G_R(E)$ and $\xi(E)$ with classical forms and considered $S_{jj',ll'}(E) = 1$, in other words, $\theta' = 0$. Therefore, to evaluate the impact of classical forms of functions $G_R(E)$ and $\xi(E)$, this section first sets the condition $\theta' = 0$ in the improved model. By comparing collision cross sections derived from this approach with those from the simplified model, we assess the influence range of such simplifications on results. After that, an investigation is conducted on the influence of θ' on collision cross sections. Subsequently, we analyze the influence of the transition quantum number Δj on the results to determine reasonable upper truncation limits for summations in the calculations. Building upon this foundation, we introduce the fitting method for θ' and construct a comprehensive improved model using the fitted θ'.

A. Analysis of simplifying assumptions

In the simplified model, classical approximations were used for $G_R(E)$ and $\xi(E)$. However, in the improved model, the complete expressions for these two functions were kept to enhance the physical accuracy of calculations. To investigate the limits of applicability for the simplified model with respect to different types of gas collisions, we compared the trends in the collision cross sections within the two models.

Figure 1 presents the collision cross section σ_R for four collision types as a function of rotational quantum number j at a relative translational energy $\varepsilon/k_B = 8000$ K and various vibrational states. For all collision types, as the rotational energy level increases, the collision cross sections for both models exhibit a gradually decreasing trend. However, the agreement between simplified and improved models varies depending on the collision type. For atom-molecule collisions, the collision cross sections under the simplified model are consistently higher than those of the improved model, particularly in the low energy range. This indicates that the simplified function leads to an overestimation of collision cross sections. For molecule-molecule collisions involving identical species (N_2-N_2 and O_2-O_2 collisions), the curves of the simplified and improved models show excellent agreement, suggesting that the simplified treatment of $G_R(E)$ and $\xi(E)$ has a negligible impact on symmetric molecular collision types.

Figure 2 further demonstrates the variation of the collision cross section with relative energy at a fixed rotational energy level of $j = 50$ to validate the influence of simplifications applied to the functions $G_R(E)$ and $\xi(E)$. The four subplots in Figure 2 correspond to the N_2-N, N_2-N_2, O_2-O and O_2-O_2 collisions respectively. From all collision types, the collision cross sections decrease monotonically with increasing relative energy. Notably, the collision cross sections for the ground vibrational state are significantly higher than those for excited vibrational states, while the collision cross sections of different excited vibrational states remain very close to each other at the same relative energy. For the atom-molecule collision types shown in Figures 2 (a) and (c), some differences between the simplified and improved models are observed. For the molecule-molecule collision types (N_2-N_2 and O_2-O_2 collisions, the results of both the simplified and improved models are almost identical, confirming the pattern observed in Figure 1.

We used the rigid rotor model for the rotational energy in both simplified and improved models in Figure 1 and 2. One of the purposes of calculating collision cross sections with different rotational state and relative energy in the two models is to understand the trend of collision cross section variation with rotational state and relative energy. Another purpose is to verify the influence of $G_R(E)$ and $\xi(E)$ summation simplification process. We used both rigid rotors and non-rigid rotors in the calculation of the simplified model (to save space, specific figures are not provided in this paper), and found that the results were consistent. This indicates that the use of rigid and non-rigid rotors in the simplified model has little impact on the final results. In other words, the classical forms of $G_R(E)$ and $\xi(E)$ in the simplified model have forced the calculation of rotational energy to be considered as the rigid rotor. Therefore, in Figure 3, we used non-rigid rotors in the simplified and improved models to further explore the applicability of the $G_R(E)$ and $\xi(E)$ with the classical form.

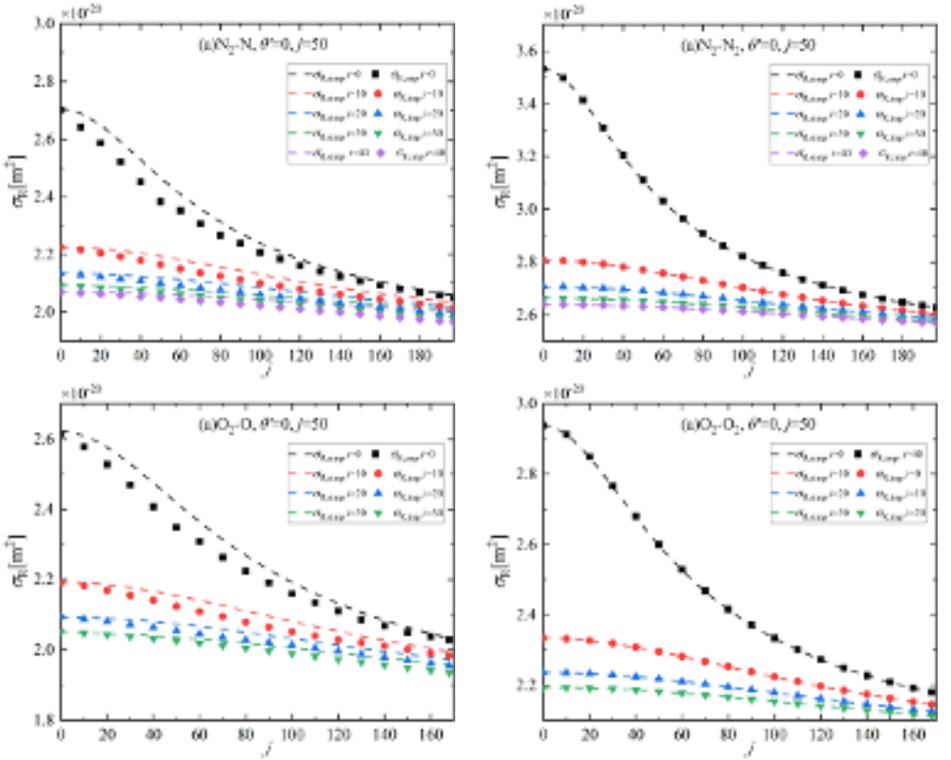

FIG. 1. The variation of collision cross sections with rotational quantum number j for different vibrational states in the two models

The collision cross section ratio between the improved and simplified models ($\sigma_{R,\mathrm{imp}}/\sigma_{R,\mathrm{simp}}$) as a function of vibrational quantum number i is examined from four different collision patterns at a relative energy of $\varepsilon/k_B = 8000$ K, as shown in Figure 3. For atom-molecule collision types, the ratio remains close to unity at low vibrational states but exhibits significant deviations at higher vibrational quantum numbers. The simplified model increasingly overestimates the collision cross-sections compared to the improved model as the vibrational excitation increases. This obvious difference at high vibrational states can be attributed to the rigid rotor approximation employed in the simplified model's treatment of $G_R(E)$ and $\xi(E)$, which becomes inadequate for highly vibrationally excited molecules where rovibrational coupling effects become substantial. For molecule-molecule collision types, the ratios remain consistently close to unity across the entire range of vibrational states examined. The maximum deviations are less than 0.2%, indicating excellent agreement between the two models. It is worth noting that for molecule-molecule interactions at the ground vibrational state, the ratio exhibits slight elevations above unity in certain rotational quantum number ranges. This phenomenon reflects the fundamental difference between the classical approximations employed in the simplified model and the complete discrete summation structures preserved in the improved model. These results validate that employing the classical form of $G_R(E)$ in the improved model is feasible for molecule-molecule collisions, as the approximation introduces negligible errors while significantly reducing computational complexity.

Therefore, when pursuing precise results, complete expressions should be adopted. For molecule-molecule collisions, such simplification barely affects the calculation results, so the simplified form can be employed to reduce computational complexity while ensuring efficiency. However, it should be noted that due to the introduction of the correlation function, $\xi(E)$ can no longer be simplified to a classical form; therefore, only the $G_R(E)$ component within $\xi(E)$ can be approximately simplified. Consequently, the collision cross-section calculation equation for molecule-molecule collisions becomes:

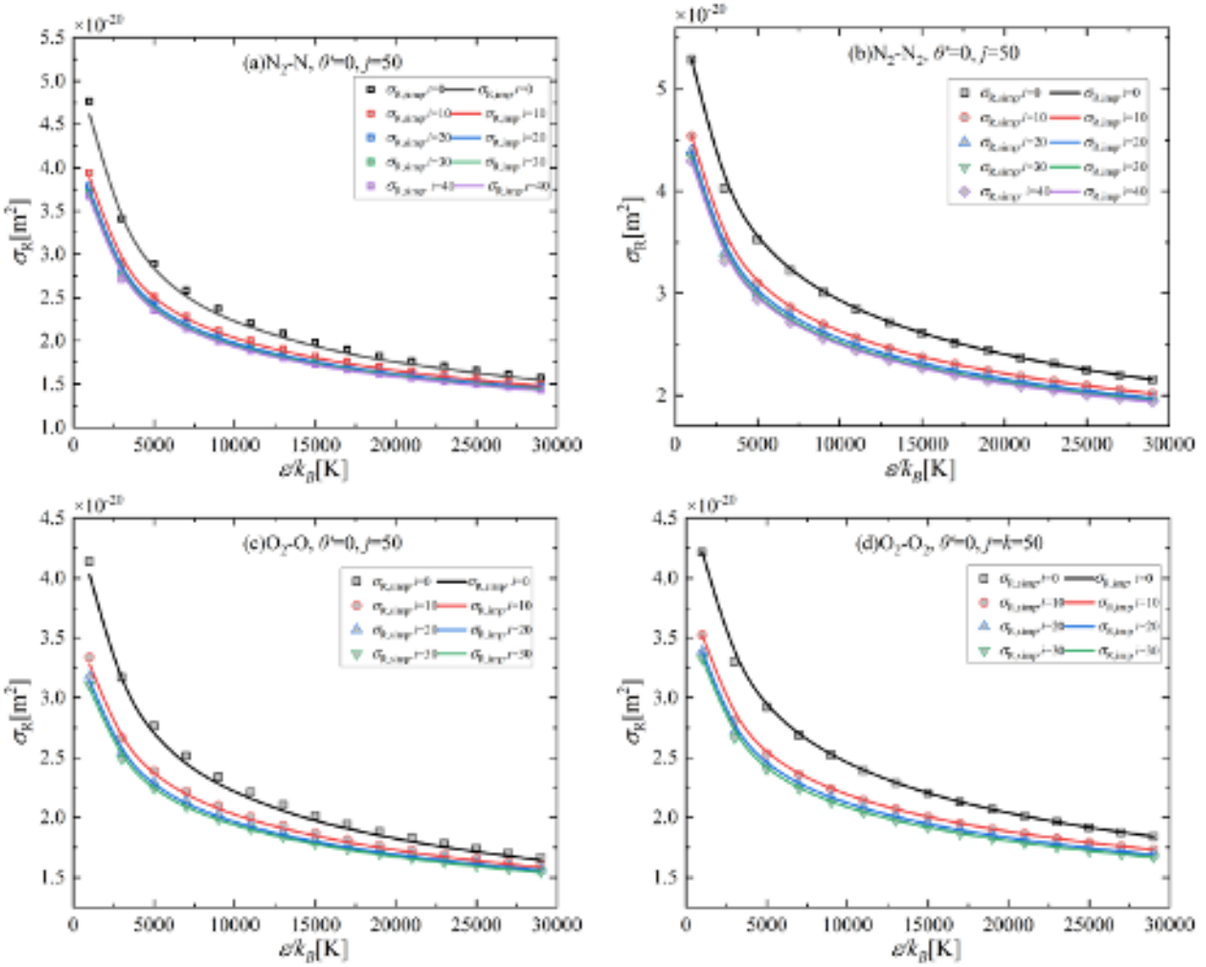

FIG. 2. The variation of collision cross sections with relative energy for different vibrational states in the two models.

$$\sigma_{\mathrm{R,imp}}(jl,\varepsilon)=\sigma_{\mathrm{el}}(\varepsilon)\left(\sum_{j'l'}\frac{2\Delta E_R(E)s_{j'}^{ci}s_{l'}^{dk}\left(E-\varepsilon_{j'}^{ci}-\varepsilon_{l'}^{dk}\right)\sigma_{\mathrm{el}}(E-\varepsilon_{j'}^{ci}-\varepsilon_{l'}^{dk})}{\{c/[2(2-\omega)(3-\omega)(4-\omega)(k_B\theta_R)^2]\}E^{4-\omega}}S_{jj',ll'}(E)\right.$$
$$\left.-\frac{2\Delta E_R(E)s_j^{ci}s_l^{dk}\left(E-\varepsilon_j^{ci}-\varepsilon_l^{dk}\right)\sigma_{\mathrm{el}}\left(E-\varepsilon_j^{ci}-\varepsilon_l^{dk}\right)}{\{c/[2(2-\omega)(3-\omega)(4-\omega)(k_B\theta_R)^2]\}E^{4-\omega}}\right). \quad (54)$$

To validate the effectiveness of the parameter θ' in the improved model, we examined its influence on collision cross sections across different collision types. Figure 4 illustrates how varying θ' affects the collision cross section as a function of relative energy at a fixed rotational energy level of $j = 50$. The results demonstrate a clear inverse relationship between θ' and collision cross sections. As θ' increases, the collision cross sections progressively decrease across all energy ranges examined. This behavior confirms the physical significance of θ' as a controlling parameter for intermolecular energy transfer processes. When $\theta' = 0$, corresponding to the absence of correlation effects in the energy transition probability, the collision cross sections attain their maximum values. Conversely, higher θ' generates greater constraints on energy transfer between molecules, thereby reducing the probability of successful collisions and resulting in diminished cross sections.This systematic variation pattern is consistently observed in both N_2-N and O_2-O systems, validating the universal applicabil-

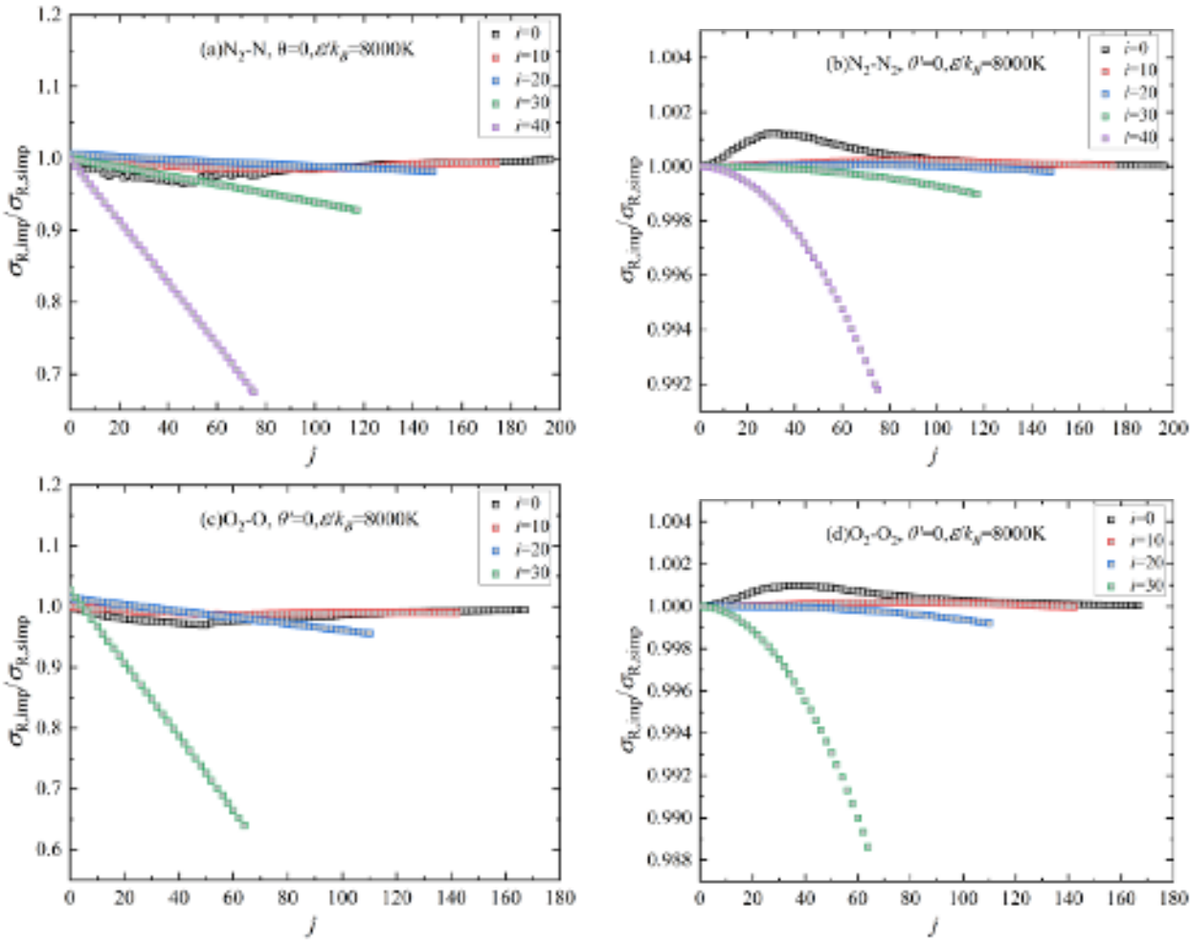

FIG. 3. The variation of $\sigma_{\mathrm{R,imp}}/\sigma_{\mathrm{R,simp}}$ with rotational quantum number j for different vibrational states.

ity of the θ' across different molecular species, though the magnitude of influence may vary between systems.

Figure 5 shows the relationship between collision cross section and relative energy in the N_2-N, N_2-N_2, O_2-O, and O_2-O_2 collisions, as well as the effect of the number of quanta $\Delta j = j' - j$ taken into account in multi-quantum transitions in the improved model on the collision cross section. All figures display the calculation results of simplified and improved models under the conditions of $\theta' = 0$ and fixed rotational energy level $j = 50$. The collision cross sections of the N_2-N and O_2-O collisions exhibit a clear monotonic decreasing trend as the relative energy ε increases. For the improved model, when Δj increases, the collision cross sections gradually increase and tend to converge. For the N_2-N systems, when $\Delta j \geq 60$, the differences between the collision cross-section curves become very small and is same as the value of simplified model, indicating that a truncation value of $\Delta j = 60$ can be selected as a reasonable upper limit for the number of quanta in multi-quantum jumps. For the O_2-O systems, convergence is achieved when $\Delta j \geq 70$, suggesting a slightly higher truncation requirement. This finding helps to reduce computational complexity while ensuring calculation accuracy.

The comprehensive analysis results demonstrate that in molecule-molecule collisions (N_2-N_2 and O_2-O_2), employing the classical form of approximation for the $G_R(E)$ and $\xi(E)$ functions yields good accuracy, introducing errors less than 0.2% while significantly reducing computational complexity. Through convergence analysis, reasonable upper truncation limits for the number of quanta in multi-quantum transitions are determined to be $\Delta j = 60$ for N_2-N systems and $\Delta j = 70$ for O_2-O systems, which requires a slightly higher truncation requirement. Furthermore, non-rigid rotor models should be adopted for rotational energy calculations, particularly as the inadequacy of rigid rotor approximations becomes more obvious at highly vibrationally excited states. These findings establish an important foundation for subsequent parameter fitting and the construction of the complete improved model.

B. Validation of improved model

Rotational energy transfer in molecular collisions follows the energy gap law. Polanyi and Woodall[29] first proposed that

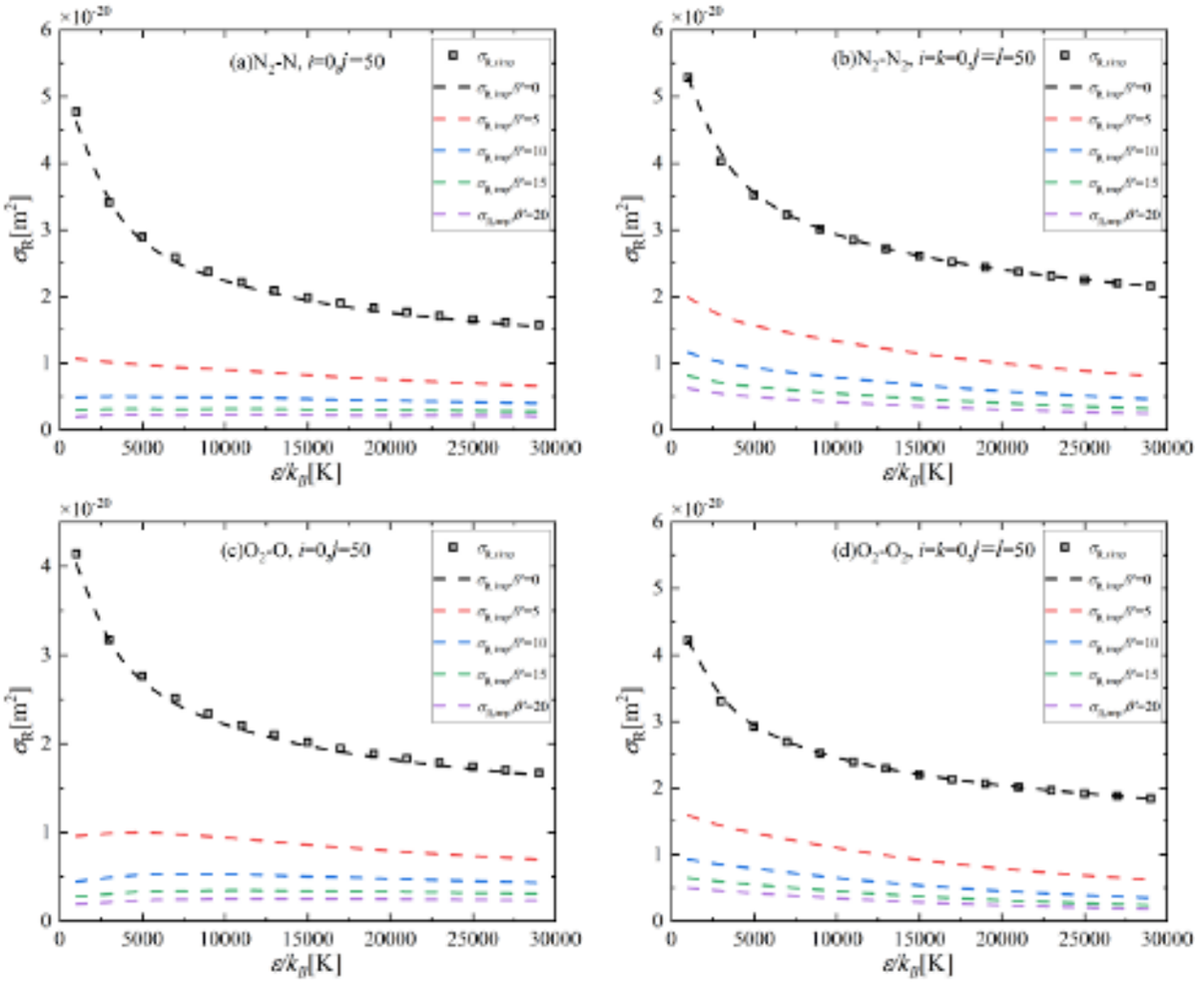

FIG. 4. The variation of collision cross sections with relative energy for different θ'.

rotational transition probabilities exhibit an exponential relationship with energy differences, subsequently Levine[30] developed the information theory-based linear surprisal model. The development of this theoretical framework has experienced an important evolution from empirical observations to microscopic theoretical foundations. Heller[31] first provided theoretical derivation for the exponential gap law from a microscopic dynamics perspective through semiclassical methods, establishing a quantitative relationship between the surprisal parameter and potential range parameter and reduced mass. Alexander et al.[25] further validated the applicability of these energy gap models in polar molecule collisions, emphasizing the importance of parameter fitting through experimental data or theoretical calculations.

With the continuous improvement of theory, Procaccia and Levine[32] developed a comprehensive approach combining classical trajectory method and information theory, providing systematic methods for parameter determination through maximum entropy principles and sum rules. Sanctuary[33] proposed a modified exponential model to improve the description of nonlinear surprisals, addressing the limitations of traditional models. Although methods for direct prediction of model parameters have been proposed, accurate parameter values can generally only be obtained through fitting, and these fitted parameters have significant physical meanings that can be used to compare different collision types and extrapolate to different conditions.This study adopts a similar energy transition model to describe the transition processes between rotational states:

$$S_{jj',ll'}(E) = \exp\left(-\theta' |\Delta E| / E\right). \tag{55}$$

This model includes the fundamental physical principle that transition probabilities decay exponentially with increasing energy gaps under energy conservation constraints.

Through systematic analysis of the averaged rotational relaxation time as a function of θ' at different temperatures, we discovered a significant linear relationship pattern as demonstrated in Figure 6. This finding reveals that the averaged rotational relaxation time exhibits a linear dependence on the parameter θ' across all temperature ranges examined, which

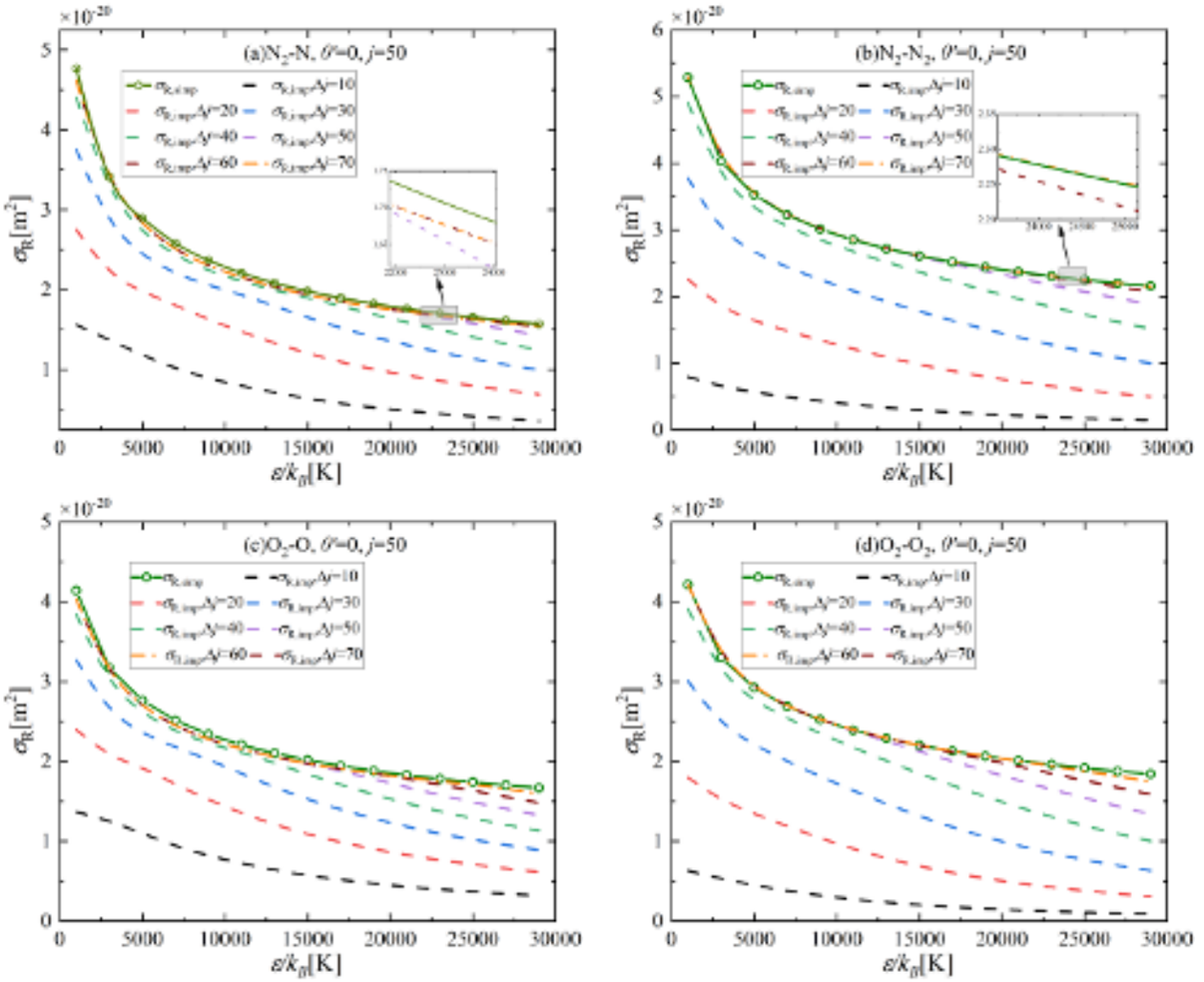

FIG. 5. The variation of collision cross sections with relative energy for different Δj in the two models.

substantially simplifies the parameter fitting procedure.

For a given temperature T, the averaged rotational relaxation time τ_{cd}^{rot} exhibits the following linear relationship with θ':

$$\tau_{cd}^{\mathrm{rot}}(T,\theta') = A(T)\cdot\theta' + B(T). \tag{56}$$

where $A(T)$ is the temperature-dependent slope coefficient, and $B(T)$ is the temperature-dependent intercept, which equals $\tau_{cd}^{\mathrm{rot}}(T,\theta'=0)$.

Based on this linear relationship, the parameter fitting process can be implemented as following:

Step 1: Initial Calculation. Calculate the averaged rotational relaxation time at $\theta'=0$:

$$\tau_{cd}^{\mathrm{rot}(0)}(T) = \tau_{cd}^{\mathrm{rot}}(T,\theta'=0). \tag{57}$$

Step 2: Trial Point Calculation. Select an arbitrary trial value θ'_{trial} and calculate the corresponding averaged rotational relaxation time:

$$\tau_{cd}^{\mathrm{rot(trial)}}(T) = \tau_{cd}^{\mathrm{rot}}(T,\theta'_{\mathrm{trial}}). \tag{58}$$

Step 3: Linear Relationship Establishment. The slope coefficient can be determined as:

$$A(T) = \frac{\tau_{cd}^{\mathrm{rot(trial)}}(T) - \tau_{cd}^{\mathrm{rot}(0)}(T)}{\theta'_{\mathrm{trial}} - 0} = \frac{\tau_{cd}^{\mathrm{rot(trial)}}(T) - \tau_{cd}^{\mathrm{rot}(0)}(T)}{\theta'_{\mathrm{trial}}}. \tag{59}$$

Step 4: Target Parameter Determination. Given the reference (theoretical or experimental) value $\tau_{cd}^{\mathrm{rot(ref)}}(T)$ at temperature T, the optimal θ' can be directly calculated:

$$\theta'_{\mathrm{opt}}(T) = \frac{\tau_{cd}^{\mathrm{rot(ref)}}(T) - \tau_{cd}^{\mathrm{rot}(0)}(T)}{A(T)}. \tag{60}$$

Substituting the expression for $A(T)$ yields

$$\theta'_{\mathrm{opt}}(T) = \frac{\tau_{cd}^{\mathrm{rot(ref)}}(T) - \tau_{cd}^{\mathrm{rot}(0)}(T)}{\tau_{cd}^{\mathrm{rot(trial)}}(T) - \tau_{cd}^{\mathrm{rot}(0)}(T)}\cdot\theta'_{\mathrm{trial}}. \tag{61}$$

To validate and fit the parameter θ', this study employs the work of Jo et al.[9,34] and Venturi et al.[23] as the primary theoretical basis. Jo et al.[9] conducted detailed state-to-state kinetic

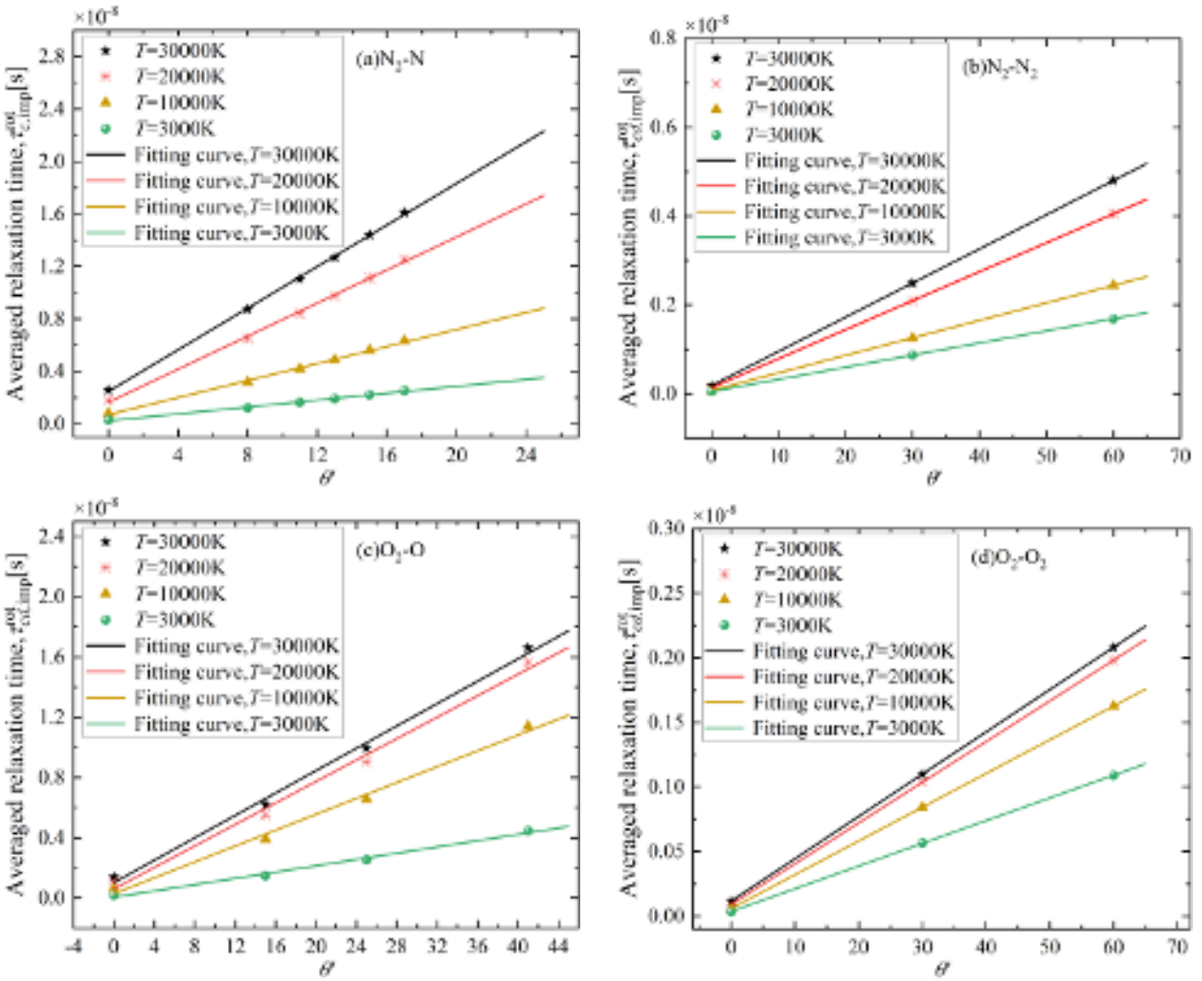

FIG. 6. The variation of averaged relaxation time with θ' and fitting curves for different temperatures.

analyses for the rotational relaxation times of N_2-N_2 and N_2-N collisions in their work on shock standoff distance prediction in air mixtures. For O_2-O_2 collisions, Jo et al.[34] employed QCT method and master equation analyses to construct a rovibrational-specific kinetic database, covering a temperature range of 7500-20000 K. The rotational relaxation time comparison data for O_2-O collisions used in this study are derived from the theoretical calculations by Venturi et al.[23].

These studies provide results with high precision and reliability, not only employing advanced *ab initio* potential energy surfaces in their methods but also validating model accuracy through comparisons with experimental data. Therefore, this study adopts these results as the primary benchmark for validating and fitting the parameter θ', ensuring the physical rationality and computational accuracy of the improved model.

To specifically illustrate the calculation process of the parameter θ', this section conducts a detailed analysis using the N_2- N collision type as an example. According to the linear relationship at $T = 30000$ K shown in Figure 6 (a), we can extract key linear parameters.

From the linear fitting results, when T is equal to 30000 K, the slope coefficient $A(T) = 7.93301 \times 10^{-10}$ s and the intercept $B(T) = 2.58769 \times 10^{-9}$ s.

According to the theoretical calculation results of Jo et al.[9] for the N_2-N collision type, the reference rotational relaxation time at $T = 30000$ K is:

$$\tau_{\mathrm{rot},c}^{(\mathrm{ref})}(30000\mathrm{K}) = 1.57985 \times 10^{-8}\ \mathrm{s}, \tag{62}$$

Applying the linear relationship method, the optimal θ' can be directly calculated through the following equation:

$$\theta'_{\mathrm{opt}}(30000\mathrm{K}) = \frac{\tau_{\mathrm{rot},c}^{(\mathrm{ref})}(30000\mathrm{K}) - \tau_{\mathrm{rot},c}^{(0)}(30000\mathrm{K})}{A(30000\mathrm{K})}, \tag{63}$$

Substituting the specific values we obtain:

$$\theta'_{\mathrm{opt}}(30000\mathrm{K}) = \frac{1.57985 \times 10^{-8} - 2.58769 \times 10^{-9}}{7.93301 \times 10^{-10}} = 16.653. \tag{64}$$

This calculation process demonstrates the efficiency of the linear relationship method: the optimal parameters can be

TABLE II. Optimal θ' for different collision types.

Collision type	N_2-N	N_2-N_2	O_2-O	O_2-O_2
θ'	16.65	821.37	34.14	696.92

accurately determined through only two calculation points ($\theta' = 0$ and $\theta' = \theta'_{\text{trial}}$), avoiding the complexity and uncertainty of traditional iterative methods.

Through the above method, we can obtain the optimal parameters θ' for different systems as shown in the Table II. The optimal θ' values determined for different collision types reveal significant variations that reflect the underlying physics of energy transfer processes. The parameter θ' quantifies the degree to which actual collision cross sections deviate from purely statistical predictions, serving as a measure of dynamical constraints in rotational energy transfer.

These differences are fundamentally physical in nature, though the parameter remains phenomenological and difficult to predict from first principles.

By substituting the optimal θ' obtained in Table II into the expression for the average rotational relaxation time, the rotational relaxation behavior of different collision types can be predicted over a wide temperature range. To validate the accuracy and universality of these parameters, we conducted systematic comparisons between our calculated results and the other theoretical data. Figure 7 presents the validation results for the N_2-N collision type, which includes theoretical data for N_2-N and N_2-N_2 collisions from the study by Jo et al.[9]. As observed in the figure, the average rotational relaxation times calculated using the optimal θ' maintain excellent consistency with the reference data throughout the entire temperature range. For the N_2-N collision, the average relative error between the calculated and reference values is only 0.61% within the temperature range of 7500-20000 K; for the N_2-N_2 collisions , the corresponding error is 0.68%. This high degree of agreement fully demonstrates the accuracy of the θ' fitting method. Similar validation results are also confirmed in O_2-O and O_2-O_2 collisions. The average relative error between calculated results and theoretical values for O_2-O collisions is 0.37%, while for the O_2-O_2 system it is 0.52%, based on comparisons with data from the study by Jo et al.[34] on oxygen mixtures. These results indicate that the improved model not only performs excellently in nitrogen systems but also demonstrates good predictive capability in oxygen systems.

IV. RESULT AND DISCUSSION

The preceding section has successfully established and validated improved rotational relaxation time models for N_2-N and O_2-O systems through comprehensive parameter sensitivity analysis. The optimal correlation function parameters were determined through systematic fitting against recent theoretical data. The validation results demonstrate excellent agreement with other calculations.

Based on this validated theoretical framework, this section presents comprehensive computational results for collision integrals and rotational relaxation times under various thermodynamic conditions. The calculations encompass a wide temperature range representative of hypersonic flow environments, from moderate heating conditions to extreme high-temperature regimes encountered in atmospheric reentry and shock wave phenomena. Additionally, the analysis extends to multiple vibrational quantum states to capture the complete spectrum of molecular energy distributions in non-equilibrium gas dynamics. It should be noted that in the previous calculations (Figures 1, 2, and 3), θ' in the improved model was set to zero in order to analyze the impact of the classical form $G_R(E)$ simplification process on collision systems. However, in the calculations of this section, we use the realistic θ' values to investigate the variation of collision integral and rotational relaxation time with vibrational states and temperature, based on the improved model.

The first subsection focuses on the computation of collision integrals for rotational energy transfer, providing detailed analysis of how these fundamental transport properties vary with temperature and vibrational states for both simplified and improved models with realistic θ'. These collision integrals serve as the foundation for macroscopic transport coefficient calculations.

The second subsection presents calculations of rotational relaxation times as functions of temperature and vibrational states for both simplified and improved models. Particular attention is given to the influence of vibrational excitation on rotational energy transfer rates, as this coupling becomes increasingly important at elevated temperatures where multiple internal energy modes are simultaneously activated. The averaged rotational relaxation times are computed and compared with existing theoretical data to assess the predictive capability of the developed models.

A. Collision integral for rotational energy transfer

Figure 8 presents the variation of collision integrals for rotational energy transfer (Q_r) as a function of vibrational quantum number i at a fixed temperature of $T = 5000$ K for four different collision types. The red solid lines represent the improved model ($Q_{r,\text{imp}}$), while the blue dashed lines represent the simplified model ($Q_{r,\text{simp}}$). For atom-molecule collision types (N_2-N and O_2-O), the values from the improved model are obviously lower than those from the simplified model. This is because the improved model uses the realistic θ' values, which reduces the probability of large quantum transitions occurring, and resulting in smaller Q_r. However, both models show similar trends in collision integrals with vibrational states, occurring slight variations at low vibrational states and significant differences occur at higher vibrational quantum numbers, where both models exhibit obvious decreasing trends, reflecting the enhanced rovibrational coupling effects at highly vibrationally excited states. For molecule-molecule collision types (N_2-N_2 and O_2-O_2), the two models show significant differences throughout the wide vibrational state range. Due to the introduction of correlation functions and realistic θ' values, the collision integral

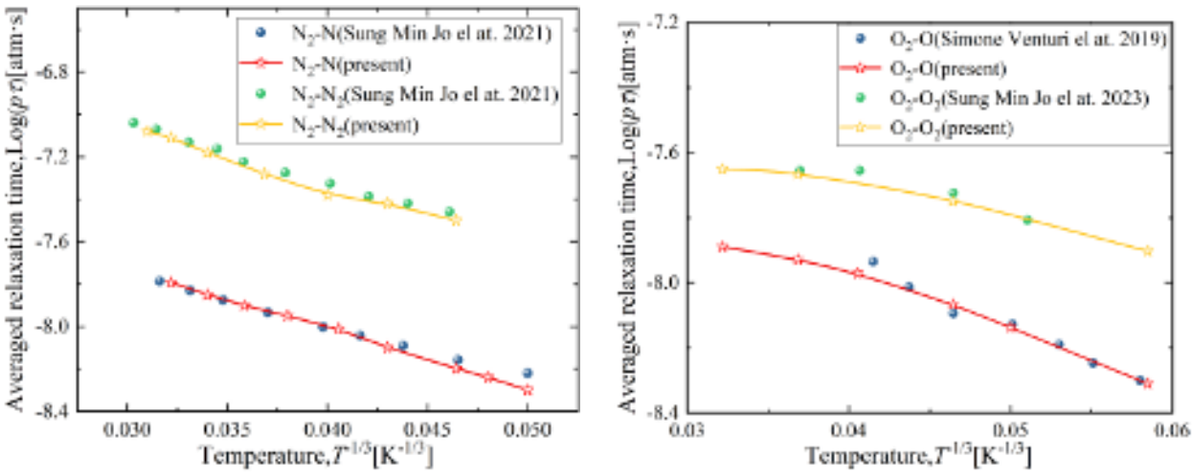

FIG. 7. The validation of optimal θ' for N_2-N and O_2-O systems with existing theoretical data.

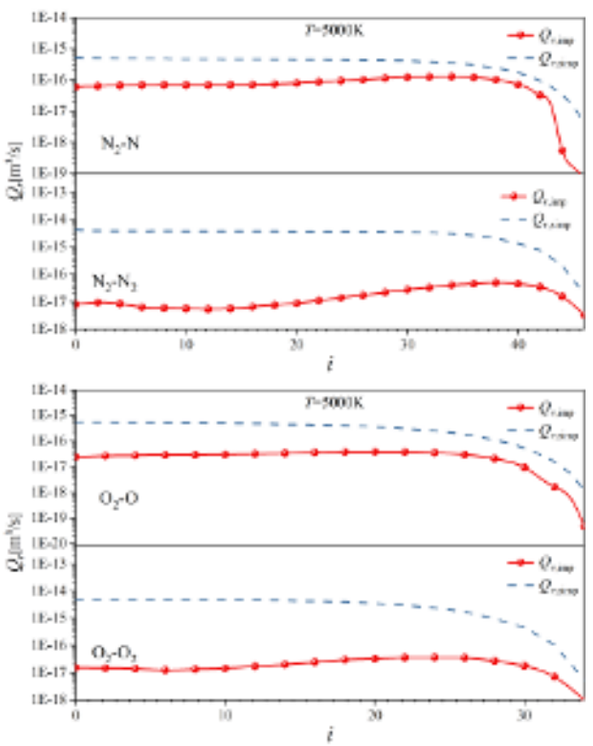

FIG. 8. The variation of Q_r with vibrational states in the two models when T = 5000K.

obtained within the improved model is not only lower than that for the simplified model, but also exhibits distinct non-monotonic behavior with vibrational states, while using the simplified model yields a monotonic decreasing trend. These results emphasize the importance of considering complete quantum state transition probabilities and correlation functions for accurately describing rotational energy transfer processes in molecule-molecule collisions.

At the temperature of $T = 30000$ K (Figure 9), the collision integrals for rotational energy transfer exhibit similar overall patterns to those observed at $T = 5000$ K, with the simplified model showing a gradual decline followed by a sharp drop at both low and high temperatures, and consistently yielding higher values than the improved model. The improved model exhibits non-monotonic behavior at low temperature but follows trends consistent with the simplified model at high temperature. The differences between the two models become more obvious at low vibrational states.

Figure 10 presents the variation of collision integrals for rotational energy transfer using the improved model ($Q_{r,imp}$) as a function of vibrational quantum number i under different temperatures for four collision types. The horizontal axis represents the vibrational state, while the vertical axis shows the collision integral values. Different colored curves correspond to various temperatures.

For all four collision types, the collision integrals consistently decrease with increasing temperature, with the highest values observed at $T = 5000$ K and the lowest at $T = 30000$ K. All systems exhibit non-monotonic behavior with respect to vibrational states at lower temperatures, showing peaks or oscillatory patterns rather than simple monotonic trends.

Distinct characteristics are observed for different collision types. For atom-molecule collisions (N_2-N and O_2-O), at temperatures below 10000 K, N_2-N collisions exhibit a more prominent single peak around $i = 35$, while O_2-O collisions show a more prominent single peak around $i = 20$. At temperatures above 10000 K, $Q_{r,imp}$ decreases monotonically with increasing vibrational states. For molecule-molecule collisions (N_2-N_2 and O_2-O_2), the behavior is markedly different, exhibiting more complex oscillatory patterns and multiple local maxima throughout the vibrational state range. The N_2-N_2 system shows particularly obvious oscillations with a dominant peak around $i = 30-35$, while the O_2-O_2 system exhibits similar oscillatory behavior. These differences highlight the increased complexity of energy transfer mechanisms in symmetric molecule-molecule interactions compared to asymmet-

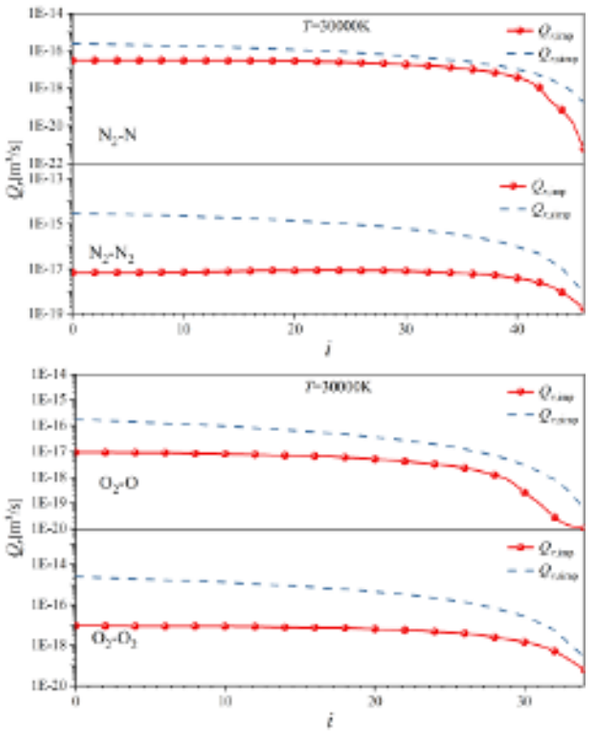

FIG. 9. The variation of Q_r with vibrational states in the two models when T = 30000K.

ric atom-molecule collisions.

B. Rotational relaxation time

Figure 11 presents the variation of rotational relaxation time with the number of rotational quanta allowed in multi-quantum transitions Δj for different vibrational states and for both simplified and improved models. The horizontal axis represents Δj, while the vertical axis shows the logarithm of rotational relaxation time. Solid lines correspond to the simplified model, and dashed lines represent the improved model. Different colors indicate various vibrational states, ranging from the ground state ($i = 0$) to highly excited states.

The overall trend for all four collision types demonstrates that rotational relaxation times decrease monotonically with increasing Δj and gradually approach convergence at higher numbers of rotational quanta taken into account in multi-quantum transitions. As Δj increases, more rotational transition combinations are considered in the calculations, requiring longer computational time but yielding more accurate results. However, beyond a certain threshold, further increases in Δj have negligible impact on the relaxation times, indicating that computational convergence has been achieved. In the simplified model, relaxation times under different vibrational states are relatively similar. However, in the improved model, different collision types exhibit distinct behaviors with respect to Δj variations. For atom-molecule collisions, rotational relaxation times for various vibrational states are relatively similar at low multi-quantum jump numbers Δj, while significant differences occur among vibrational states at high Δj. For molecule-molecule collisions, some vibrational states already show differences in rotational relaxation times even at low Δj. Convergence is achieved when $\Delta j \geq 60$ for both models in the N_2-N system. For the O_2-O system, convergence is reached when $\Delta j \geq 70$ for both models.

These convergence values are consistent with the collision cross-section analysis presented in Section III, confirming the reliability of the established truncation limits for practical computational applications. Based on these convergence analysis results, in all subsequent calculations, $\Delta j = 60$ is adopted for N_2-N and N_2-N_2 collision types, while $\Delta j = 70$ is used for the O_2-O collision type to ensure computational accuracy while optimizing computational efficiency. The systematic convergence behavior validates the computational methodology and provides clear guidelines for balancing accuracy and efficiency in rotational relaxation time calculations.

Figure 12 presents the variation of rotational relaxation time with temperature for different vibrational states in both simplified and improved models. The horizontal axis represents the inverse temperature ($T^{-1/3}[K^{-1/3}]$), while the vertical axis shows the logarithm of rotational relaxation time. Solid lines correspond to the simplified model, and dashed lines represent the improved model. In the simplified model, the variation of rotational relaxation times with temperature for different vibrational states is highly consistent and monotonic, and at the same temperature, rotational relaxation times for different vibrational states are relatively similar. However, in the improved model, different collision types exhibit significantly different behaviors in how rotational relaxation times for various vibrational states vary with temperature, with obvious numerical differences. The relaxation times of the improved model are consistently higher than those of the simplified model, primarily because the improved model considers transition probabilities between rotational energy levels. For atom-molecule collision types (Figures12 (a) and (c)), both N_2-N and O_2-O exhibit strong temperature dependence, particularly for lower vibrational states. The ground vibrational state ($i = 0$) shows the most obvious temperature sensitivity, with relaxation times varying by nearly two orders of magnitude across the examined temperature range. In the improved model, higher vibrational energy levels correspond to shorter rotational relaxation times. In contrast, molecule-molecule collision types (Figures 12 (b) and (d)) display markedly different behavior. For N_2-N_2 and O_2-O_2 collisions, both simplified and improved models show smaller variations with temperature across all vibrational states and are not strictly monotonic. Compared to atom-molecule systems, the temperature dependence is less obvious, and the influence of vibrational excitation on temperature sensitivity is minimal.

Figure 13 presents a comparison of rotational relaxation times between the improved and simplified models developed in this study and existing theoretical data from the study for N_2-N and O_2-O systems. In Figure 13 (a), the improved model of this study (red solid line) demonstrates excellent agreement with the computational results of Jo et al.[9], Macdonald et

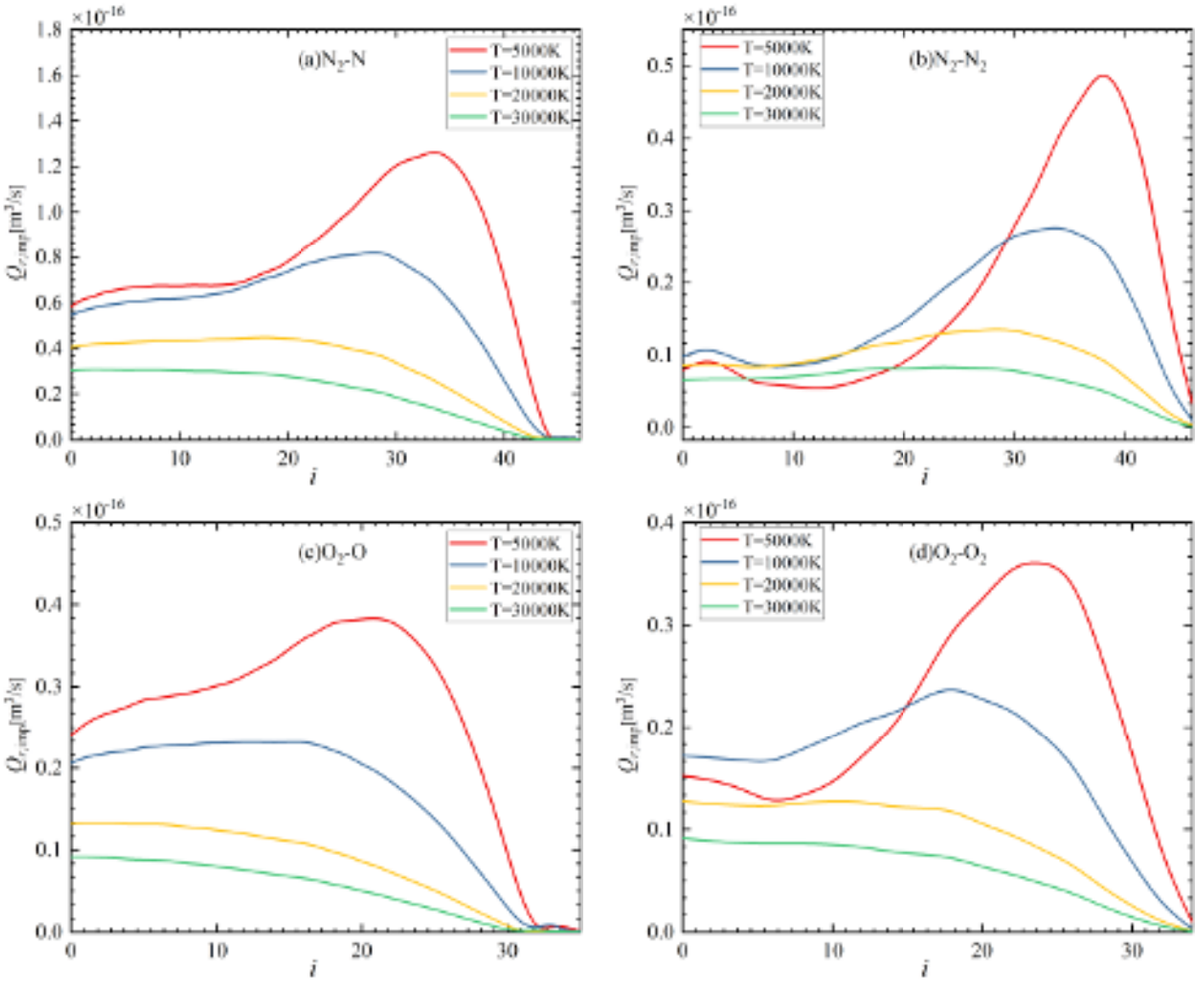

FIG. 10. The variation of $Q_{r,\mathrm{imp}}$ with vibrational states for different temperatures.

al.[35], Kim and Boyd[13] across the large temperature range. Jo et al.[9] employed an innovative atomistic QCT approach that separates rotational and vibrational energy modes from coupled rovibrational states, assuming vibrational states follow a Boltzmann distribution at vibrational temperature, thereby significantly reducing computational cost while calculating complete rotational state-to-state transition rates based on *ab initio* N_3 potential energy surfaces. Kim and Boyd[13] used complete state-to-state transition rates from the NASA Ames database containing 9,390 rovibrational states, establishing comprehensive master equation systems to describe bound-bound, bound-free, and predissociation transition processes. Macdonald et al.[35] developed a coarse-grain QCT method that balances computational accuracy and efficiency by grouping rovibrational states, with detailed validation through comparison with direct molecular simulation methods. The improved model of this study exhibits excellent consistency with these three studies based on modern *ab initio* potential energy surfaces and detailed state-to-state dynamics across the large temperature range. This close agreement validates the accuracy of the proposed methodology and confirms that the introduction of exponential correlation functions provides a physically realistic representation of rotational energy transfer processes in atom-molecule collisions. The Parker model[19] predictions are significantly higher, showing substantial deviation from these advanced models. It is derived based on rigid rotor assumptions and hard sphere collision models, and this simplified treatment cannot accurately describe the complex intermolecular interactions and rovibrational coupling effects, particularly at high temperatures where the limitations of the rigid rotor assumption become more obvious. Meanwhile, the simplified model of this study exhibits systematic deviation from the reference data, consistently predicting longer relaxation times, especially at higher temperatures. This discrepancy highlights the limitations of simplified approximations when applied to atom-molecule collision types where rovibrational coupling effects become significant.

Based on the validated improved rotational relaxation time model described above, Figure 13 (b) presents a comparison of rotational relaxation times between the present simplified

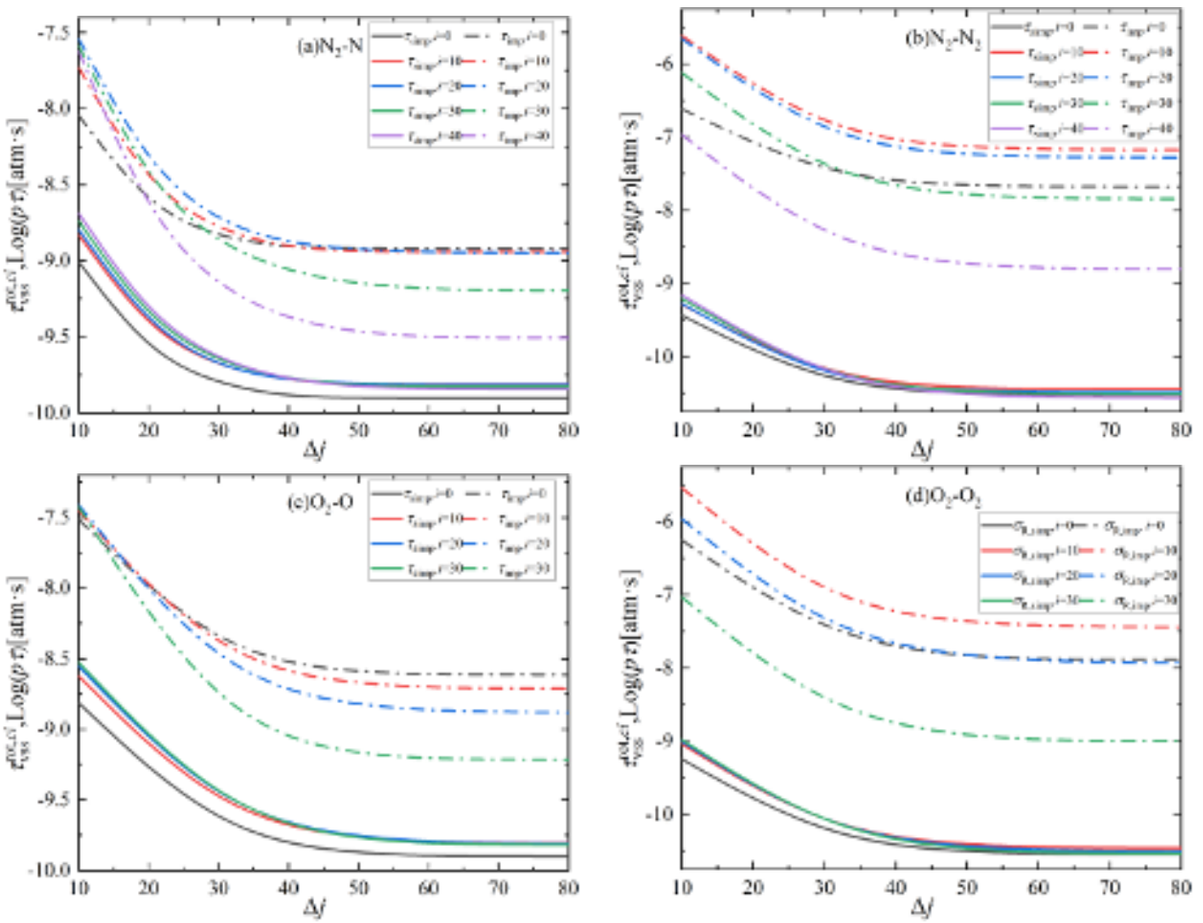

FIG. 11. The variation of rotational relaxation time with Δj for different vibrational states in the two models.

and improved models and existing theoretical data from the study for the N_2-N_2 collision type. The figure covers a wide temperature range from moderate to extremely high temperatures, with comparisons including the master equation calculations and curve-fitting results from Jo et al.[9], theoretical calculations from Park[36], and predictions from the classical Parker model[19].

In the work by Jo et al.[9], an innovative rovibrational separation approach and QCT calculations based on *ab initio* N_4 potential energy surfaces were employed to determine the rotational relaxation time for N_2-N_2 collisions through rotational state-resolved master equations. This method[9] assumes that vibrational states follow a Boltzmann distribution at the vibrational temperature, successfully avoiding the computational challenge of handling 10^{15} rovibrational state combinations while maintaining accuracy in physical description. Park's work[36] was based on the empirical equation of Rahn and Palmer, boldly extrapolating low-temperature experimental data ($\leq$1500K) to high-temperature ranges up to 128,000K. The Parker model[19] employs rigid rotor assumptions and hard sphere gas models to describe molecular collision processes, which, while computationally convenient, has a relatively simplified physical foundation. Significant differences exist among the various models, primarily because of their different theoretical foundations and assumptions. Park's model predicts significantly higher relaxation times at high temperatures compared to other models, with this deviation mainly attributed to uncertainties in its extrapolation method. Park's model involves substantial extrapolation based on experimental data below 1500K, and at high temperatures, the rotational relaxation time even exceeds the vibrational relaxation time, which is considered "hypothetical" from a physical viewpoint because rovibrational coupling effects would cause the temperatures of these two modes to converge. The Parker model's predictions are moderate but lack temperature dependence, as this model is derived based on rigid rotor assumptions and cannot accurately describe quantum mechanical effects and the influence of internal molecular structure on energy transfer processes at high temperatures. The present simplified model, due to overly simplified assumptions, particularly in the treatment of quantum energy level transition probabilities, results in significantly underestimated relaxation times. The improved model determined in this study demonstrates excellent agreement with the latest theoretical calculations by Jo et al.[9], validating the accuracy and reliability of the proposed approach. The improved model

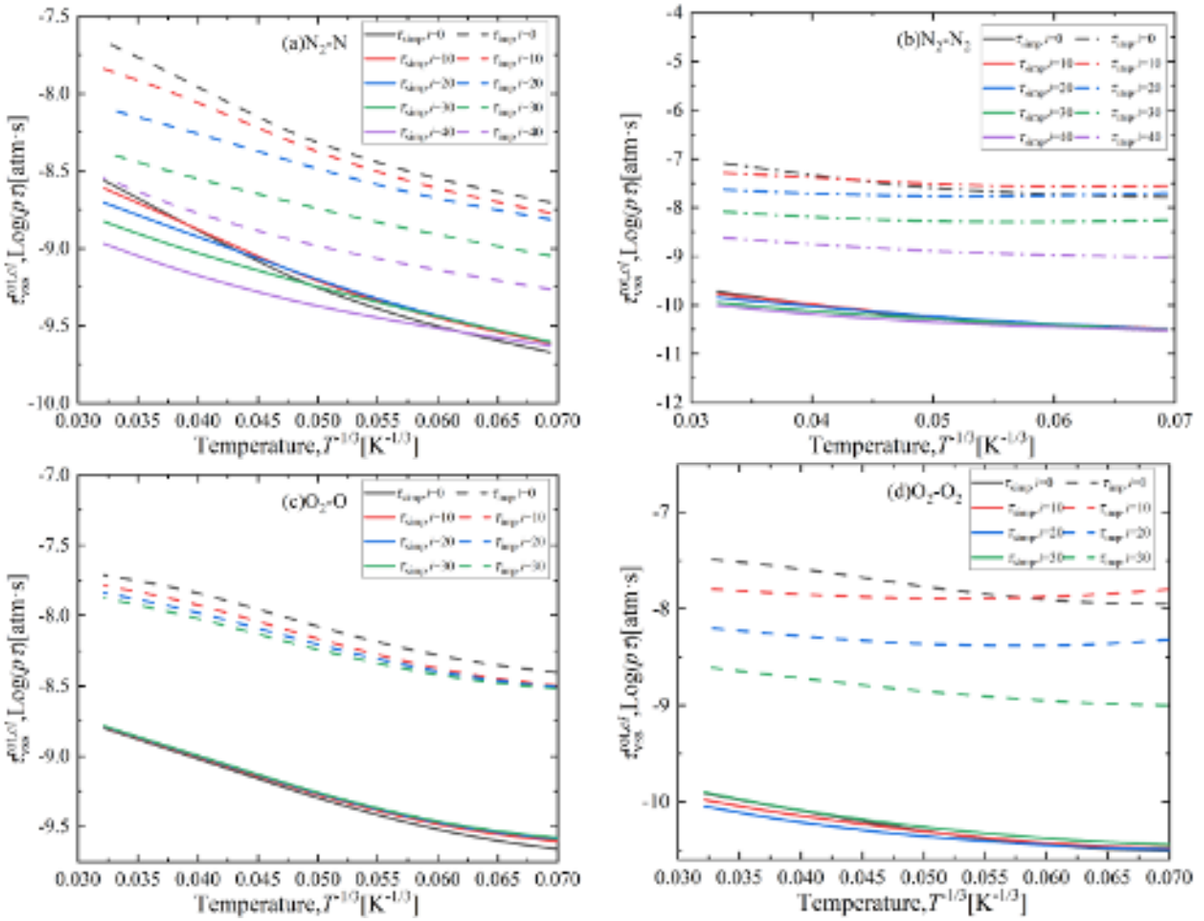

FIG. 12. The variation of rotational relaxation time with temperature for different vibrational states in the two models.

effectively describes the variation of transition probabilities with energy gaps through the introduction of the θ', overcoming the limitations of the simplified model.

Figure 13 (c) and (d) respectively show comparisons between the present calculated rotational relaxation times for O_2-O and O_2-O_2 collisions and other exciting data. In O_2-O collisions, Venturi et al.[23] employed a rotationally and vibrationally state-resolved QCT method, using nine potential energy surfaces developed by Varga et al.[37] to describe the multiplet interactions of the O_2-O system. They simulated non-equilibrium relaxation processes through the master equation method and defined relaxation times using the e-folding method. The rotational relaxation time calculations from the improved model in this study show excellent agreement with the data from Venturi et al.[23], with the curves almost completely overlapping. However, compared to the results of Andrienko and Boyd[38], there are significant differences, with their predicted relaxation times being approximately one order of magnitude higher than those in this study. This is because Andrienko and Boyd[38] used a QCT method combined with a single potential energy surface developed by Varandas and Pais[39], which is a singlet ground state potential energy surface with much lower reactivity than the quintet potential energy surface. For O_2-O_2 collisions, Jo et al.[34] adopted a thermal collider (TC) method, which assumes that the internal states of one O_2 molecule follow a Boltzmann distribution at a given internal temperature, thereby reducing the computational complexity of the four-atom system to a level comparable to that of a three-atom system. They used the QCT method combined with high-accuracy *ab initio* potential energy surfaces developed by Paukku et al.[40,41] to calculate state-to-state transition rates, then determined relaxation times through the master equation method and e-folding method. The results from the improved model show good agreement with the latest computational data from Jo et al.[34], particularly in considering temperature dependence, further confirming the accuracy of the improved model in handling complex molecule-molecule collision types. In both O_2-O and O_2-O_2 collisions, the Parker model, as a theoretical model based on classical mechanics and rigid rotor approximation, shows significant deviations in its predictions at high temperatures. The simplified model, due to neglecting quantum transition probabilities of rotational energy levels, yields calculated results much smaller than other theoretical values.

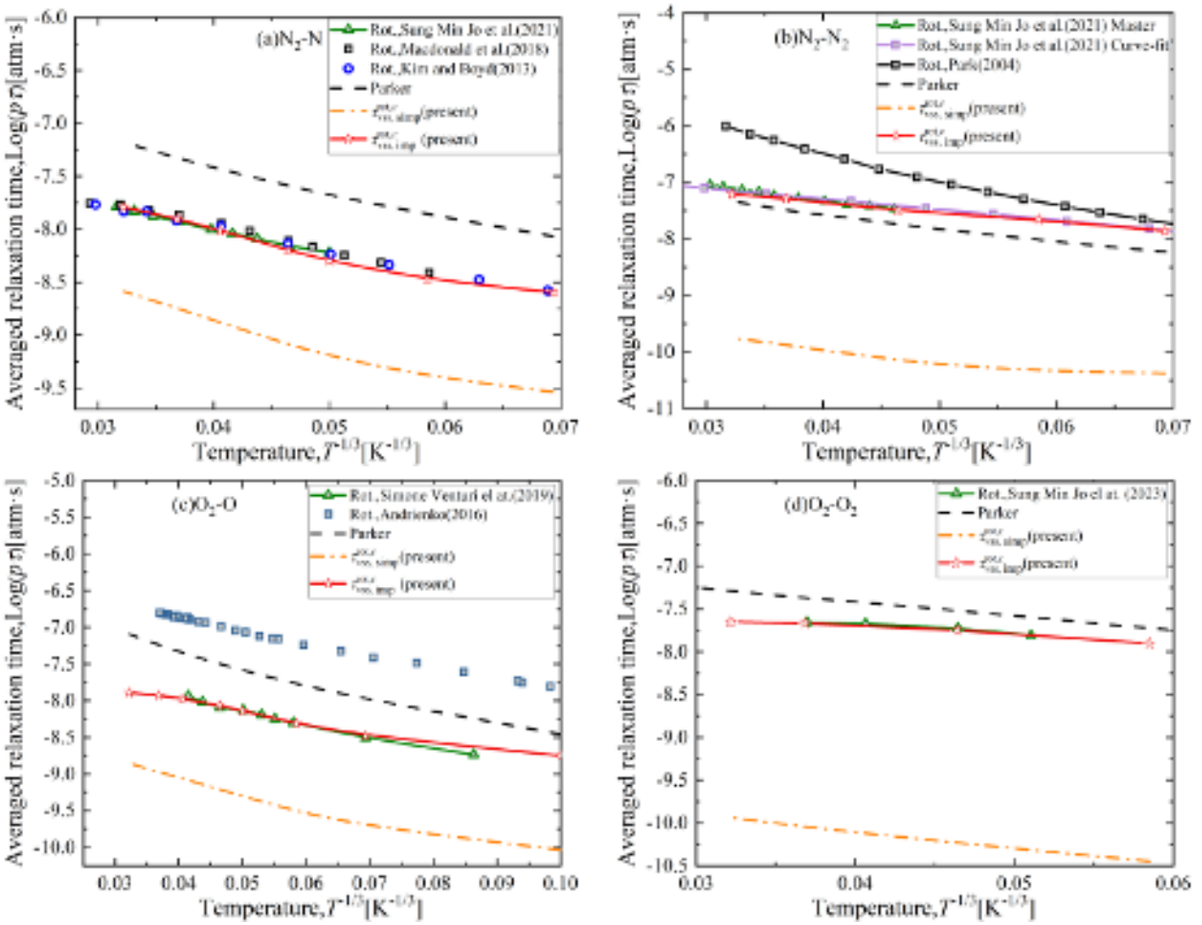

FIG. 13. Comparison of rotational relaxation times in the N_2-N and O_2-O systems with simplified model and existing theoretical data.

V. CONCLUSION

This study has successfully developed and validated an improved computational framework for vibrationally state-resolved rotational relaxation times, which, while ensuring computational efficiency, addresses the critical problem that the traditional Parker model based on rigid rotor assumptions fails to accurately describe the effects of internal molecular structure on the energy transfer processes under high-temperature non-equilibrium conditions.

An improved rotational relaxation time computational model incorporating vibrational state-resolved calculations and exponential correlation functions has been established, which includes the exponential correlation function $S_{jj',ll'}(E) = \exp(-\theta'|\Delta E|/E)$ to accurately describe transition probabilities between rotational energy levels. This model overcomes the limitations of simplified statistical models by maintaining complete summation structures and properly accounting for rovibrational coupling effects, while ensuring reasonable computational costs and enabling consideration of rotational relaxation times for each vibrational state.

Systematic parameter sensitivity analysis reveals that the averaged rotational relaxation time exhibits a linear dependence on the parameter θ', significantly simplifying the fitting procedure. Optimal θ' values were determined for key collision types: N_2-N (16.65), N_2-N_2 (821.37), O_2-O (34.14), and O_2-O_2 (696.92). Validation against recent theoretical data demonstrates that the average relative errors for all studied systems are below 0.7%.

Important computational guidelines have been established: convergence requires $\Delta j = 60$ for N_2-N systems and $\Delta j = 70$ for O_2-O systems. For molecule-molecule collisions, classical form approximations introduce negligible errors ($< 0.2\%$) while significantly reducing computational complexity. The analysis reveals that atom-molecule and molecule-molecule collision types exhibit strong sensitivity to correlation function treatments, and molecule-molecule systems display complex oscillatory behavior in collision integrals. Vibrational states significantly influence the rotational relaxation time.

The validated improved model provides a basic tool for hypersonic flow simulations, serving as fundamental input for transport coefficient calculations in computational fluid dynamics codes. However, the current study only covers four collision types: N_2-N, N_2-N_2, O_2-O, and O_2-O_2, and the pa-

rameter θ' lacks a universal analytical prediction method, requiring determination through fitting. Future research should be extended to more molecular systems and collision partners, explore the physical significance of the parameter θ' to establish a predictive theoretical framework.

ACKNOWLEDGMENT

The research leading to these results is supported by the Saint Petersburg State University, Project No. 116636233. The authors are grateful to Lei Tan for checking and improving the code.

CONFLICT OF INTEREST

The authors have no conflicts to disclose.

DATA AVAILABILITY

The data that support the findings of this study are available from the corresponding author upon reasonable request.

[1]Q.-S. He, S.-R. Sun, X. Cao, H. Jia, Y.-W. Du, and H.-X. Wang, "Non-equilibrium modeling on the aerothermodynamic characteristics of hypersonic inflatable reentry vehicle," Aerospace Science and Technology **141**, 108524 (2023).
[2]Y. V. Stupochenko, S. A. Losev, and A. I. Osipov, *Relaxation processes in shock waves* (Springer, Berlin, 1967).
[3]F. C. Moreira, W. R. Wolf, and J. L. F. Azevedo, "Thermal analysis of hypersonic flows of carbon dioxide and air in thermodynamic non-equilibrium," International Journal of Heat and Mass Transfer **165**, 120670 (2021).
[4]D. Passiatore, L. Sciacovelli, P. Cinnella, and G. Pascazio, "Thermochemical non-equilibrium effects in turbulent hypersonic boundary layers," Journal of Fluid Mechanics **941**, A21 (2022).
[5]A. I. Bechina and E. V. Kustova, "Rotational energy relaxation time for vibrationally excited molecules," Vestnik St. Petersburg University, Mathematics **52**, 81–91 (2019).
[6]M. Capitelli, C. M. Ferreira, B. F. Gordiets, and A. I. Osipov, "Rotational relaxation of molecules," in *Plasma Kinetics in Atmospheric Gases* (Springer Berlin Heidelberg, Berlin, Heidelberg, 2000) pp. 13–22.
[7]E. Kustova, M. Mekhonoshina, A. Bechina, S. Lagutin, and Y. Voroshilova, "Continuum models for bulk viscosity and relaxation in polyatomic gases," Fluids **8**, 48 (2023).
[8]Y. Zeng, "Gas dynamics in thermal nonequilibrium and general hyperbolic systems with relaxation," Archive for rational mechanics and analysis **150**, 225–279 (1999).
[9]S. M. Jo, M. Panesi, and J. G. Kim, "Prediction of shock standoff distance with modified rotational relaxation time of air mixture," Physics of Fluids **33** (2021).
[10]F. C. Moreira, W. R. Wolf, and J. L. F. Azevedo, "Thermal analysis of hypersonic flows of carbon dioxide and air in thermodynamic non-equilibrium," International Journal of Heat and Mass Transfer **165**, 120670 (2021).
[11]J. J. Shang and H. Yan, "High-enthalpy hypersonic flows," Advances in Aerodynamics **2**, 19 (2020).
[12]J. H. Chae, T. K. Mankodi, S. M. Choi, and R. S. Myong, "Combined effects of thermal non-equilibrium and chemical reactions on hypersonic air flows around an orbital reentry vehicle," International Journal of Aeronautical and Space Sciences **21**, 612–626 (2020).
[13]J. G. Kim and I. D. Boyd, "State-resolved master equation analysis of thermochemical nonequilibrium of nitrogen," Chemical Physics **415**, 237–246 (2013).
[14]E. Nagnibeda and E. Kustova, *Non-equilibrium reacting gas flows: kinetic theory of transport and relaxation processes* (Springer Science & Business Media, 2009).
[15]E. Kustova, M. Mekhonoshina, and G. Oblapenko, "On the applicability of simplified state-to-state models of transport coefficients," Chemical Physics Letters **686**, 161–166 (2017).
[16]Q. Hong, L. Storchi, Q. Sun, M. Bartolomei, F. Pirani, and C. Coletti, "Improved quantum–classical treatment of n2–n2 inelastic collisions: Effect of the potentials and complete rate coefficient data sets," Journal of chemical theory and computation **19**, 8557–8571 (2023).
[17]I. D. Boyd and T. E. Schwartzentruber, *Nonequilibrium gas dynamics and molecular simulation*, Vol. 42 (Cambridge University Press, 2017).
[18]R. Tompson and S. Loyalka, "Chapman-Enskog solution for diffusion: Pidduck's equation for arbitrary mass ratio," Physics of Fluids **30**, 2073–2075 (1987).
[19]J. Parker, "Rotational and vibrational relaxation in diatomic gases," The Physics of Fluids **2**, 449–462 (1959).
[20]S. Subramaniam, R. L. Jaffe, and K. A. Stephani, "State-resolved transport collision integrals for the O+O_2 system," Physical Review Fluids **5**, 113402 (2020).
[21]S. Subramaniam and K. A. Stephani, "Computation of state to state transport coefficients using ab initio potential energy surfaces for the O+O_2 system," in *AIAA Scitech 2019 Forum* (2019) p. 1050.
[22]Q. Hong, Q. Sun, F. Pirani, M. Valentín-Rodríguez, R. Hernández-Lamoneda, C. Coletti, M. Hernández, and M. Bartolomei, "Energy exchange rate coefficients from vibrational inelastic O_2+O_2 collisions on a new spin-averaged potential energy surface," J Chem Phys **154** (2021).
[23]S. Venturi, M. Sharma Priyadarshini, A. Racca, and M. Panesi, "Effects of ab-initio potential energy surfaces on o2-o non-equilibrium kinetics," in *AIAA Aviation 2019 Forum* (2019) p. 3358.
[24]K. Koura, "Statistical inelastic cross-section model for the Monte Carlo simulation of molecules with discrete internal energy," Physics of Fluids A: Fluid Dynamics **4**, 1782–1788 (1992).
[25]M. H. Alexander, E. F. Jendrek, and P. J. Dagdigian, "Validity of energy gap representations of rotationally inelastic cross sections between polar molecules," The Journal of Chemical Physics **73**, 3797–3803 (1980).
[26]K. Koura and H. Matsumoto, "Variable soft sphere molecular model for inverse-power-law or Lennard-Jones potential," Physics of Fluids A: Fluid Dynamics **3**, 2459–2465 (1991).
[27]E. Kustova and G. M. Kremer, "Effect of molecular diameters on state-to-state transport properties: The shear viscosity coefficient," Chem. Phys. Lett. **636**, 84–89 (2015).
[28]K. Koura and H. Matsumoto, "Variable soft sphere molecular model for air species," Physics of Fluids A: Fluid Dynamics **4**, 1083–1085 (1992).
[29]J. C. Polanyi and K. B. Woodall, "Mechanism of rotational relaxation," The Journal of Chemical Physics **56**, 1563–1572 (1972).
[30]R. Levine, R. Bernstein, P. Kahana, I. Procaccia, and E. Upchurch, "Surprisal analysis and probability matrices for rotational energy transfer," The Journal of Chemical Physics **64**, 796–807 (1976).
[31]D. F. Heller, "Exponential gap law for atom—diatom inelastic scattering," Chemical Physics Letters **45**, 64–70 (1977).
[32]I. Procaccia and R. D. Levine, "Cross sections for rotational energy transfer: An information-theoretic synthesis," The Journal of Chemical Physics **64**, 808–817 (1976).
[33]B. Sanctuary, "Energy dependence of rotational cross sections," Chemical Physics Letters **62**, 378–383 (1979).
[34]S. M. Jo, S. Venturi, J. G. Kim, and M. Panesi, "Rovibrational internal energy transfer and dissociation of high-temperature oxygen mixture," The Journal of Chemical Physics **158** (2023).
[35]R. Macdonald, R. Jaffe, D. Schwenke, and M. Panesi, "Construction of a coarse-grain quasi-classical trajectory method. i. theory and application to n2–n2 system," The Journal of chemical physics **148** (2018).
[36]C. Park, "Rotational relaxation of N_2 behind a strong shock wave," Journal of Thermophysics and Heat Transfer **18**, 527–533 (2004).
[37]Z. Varga, Y. Paukku, and D. G. Truhlar, "Potential energy surfaces for O+O_2 collisions," The Journal of chemical physics **147** (2017).

[38]D. A. Andrienko and I. D. Boyd, "Rovibrational energy transfer and dissociation in o2–o collisions," The Journal of chemical physics **144** (2016).
[39]A. Varandas and A. Pais, "A realistic double many-body expansion (dmbe) potential energy surface for ground-state o3 from a multiproperty fit to ab initio calculations, and to experimental spectroscopic, inelastic scattering, and kinetic isotope thermal rate data," Molecular Physics **65**, 843–860 (1988).
[40]Y. Paukku, K. R. Yang, Z. Varga, G. Song, J. D. Bender, and D. G. Truhlar, "Potential energy surfaces of quintet and singlet O_4," The Journal of chemical physics **147** (2017).
[41]Y. Paukku, Z. Varga, and D. G. Truhlar, "Potential energy surface of triplet O_4," The Journal of chemical physics **148** (2018).